



## RESEARCH ARTICLE

# Brain penetration of peripheral extracellular vesicles from Alzheimer's patients and induction of microglia activation

Hermine Counil<sup>1</sup>  | Rummenigge Oliveira Silva<sup>1</sup> | Jean-Michel Rabanel<sup>1,2</sup> |  
 Charlotte Zaouter<sup>1</sup> | Mohamed Haddad<sup>1</sup> | Mohamed Raâfet Ben Khedher<sup>1,3</sup> |  
 Davide Brambilla<sup>4</sup> | Tamas Fülöp<sup>5</sup> | Shunmoogum A. Patten<sup>1</sup> | Charles Ramassamy<sup>1</sup> 

<sup>1</sup>INRS, Centre Armand-Frappier Santé Biotechnologie, Laval, Quebec, Canada

<sup>2</sup>School of Pharmaceutical Sciences, Faculty of Medicine, University of Ottawa, Ottawa, Ontario, Canada

<sup>3</sup>Higher Institute of Biotechnology of Beja, University of Jendouba, Beja, Tunisia

<sup>4</sup>Université de Montréal, Faculté de Pharmacie, Pavillon Jean-Coutu, Montréal, Quebec, Canada

<sup>5</sup>Research Center on Aging, Graduate Program in Immunology, Faculty of Medicine and Health Sciences, University of Sherbrooke, Sherbrooke, Quebec, Canada

## Correspondence

Charles Ramassamy, INRS, Centre Armand-Frappier Santé Biotechnologie, 525, boulevard des Prairies, Laval, QC, Canada. Email: [charles.ramassamy@inrs.ca](mailto:charles.ramassamy@inrs.ca)

## Funding information

Research Chair Louise & André Charron on Alzheimer's disease; Foundation Armand-Frappier

## Abstract

Alzheimer's disease (AD) is an age-related neurodegenerative pathology. Brain-derived extracellular vesicles (EVs) have been demonstrated to be implicated in AD pathogenesis by facilitating the propagation of Tau, amyloid- $\beta$  and inflammatory cytokines. However, the impact of peripheral EVs (pEVs) in AD pathogenesis remains poorly investigated. The objective of our study was to compare the passage of pEVs from adults, cognitively healthy elderly, and AD patients through the blood-brain barrier (BBB), to evaluate their uptake in the brain and to assess their impact on the microglia activity using in vitro and in vivo models. To this end, pEVs were enriched, characterized, and fluorescently labelled. The passage of pEVs through the endothelial bEnd.3 cells was studied in a Transwell device with either neuronal or microglia cells seeded at the bottom of the well. Following the internalization of pEVs from AD patients, microglia adopted an amoeboid morphology and released a heightened level of pro-inflammatory cytokine IL-6. To further assess their in vivo transport across the BBB, pEVs were injected into the blood circulation of 2-days post-fertilization *Tg(flk1:EGFP)* zebrafish. The biodistribution of pEVs was monitored at 1 and 24 h post-injection using confocal microscopy. We demonstrated that pEVs traverse the BBB by transcytosis and subsequently diffuse progressively into the brain. pEVs were then internalized by neuronal and radial glial cells as seen in *Tg(huc:EGFP)* and *Tg(gfap:EGFP)* zebrafish, respectively. Additional experiments were performed with the intrahippocampal injection of pEVs in the mouse, indicating their spreading throughout the brain and their uptake by neuronal and glial cells. These findings contribute to novel insights into the fate of pEVs following their passage through the BBB in vitro and in vivo, and demonstrate for the first time that pEVs from AD patients affect microglia activity. This suggests a potential mechanism through which peripheral tissue cues may contribute to AD pathogenesis.

## KEYWORDS

Alzheimer's disease, blood-brain barrier, brain, extracellular vesicles, microglia, zebrafish

This is an open access article under the terms of the [Creative Commons Attribution-NonCommercial-NoDerivs License](https://creativecommons.org/licenses/by-nc-nd/4.0/), which permits use and distribution in any medium, provided the original work is properly cited, the use is non-commercial and no modifications or adaptations are made.

© 2025 The Author(s). *Journal of Extracellular Biology* published by Wiley Periodicals LLC on behalf of International Society for Extracellular Vesicles.

## 1 | INTRODUCTION

Alzheimer's disease (AD) is an age-related neurodegenerative disease affecting more than 55 million people worldwide with a projected prevalence of 139 million in 2050 (Gauthier, 2022). The clinical diagnosis relies on progressive cognitive impairments, memory loss and mood disorders (Hardy, 2006). The neuropathological hallmarks of AD include two misfolded proteins: the amyloid- $\beta$  peptide ( $A\beta$ ) and the phosphorylated Tau protein, associated with neuroinflammation (Hardy & Selkoe, 2002; Heneka et al., 2015). Neuroinflammation is recognized to play an instrumental role in AD pathogenesis (Heneka et al., 2015). It could precede  $A\beta$  deposition (McGeer & McGeer, 2013) and approximately two thirds of new AD-risk single-nucleotide polymorphisms were found to be expressed in microglial cells (Marioni et al., 2018), the innate and resident immune cells in the brain. In AD, microglia might have a double-edged sword role. At the early stages, it may exert a protective effect by promoting  $A\beta$  clearance, then play a detrimental role with a progressive switch from homeostatic to disease-associated microglial phenotype (Butovsky & Weiner, 2018). Microglia can spread  $A\beta$  (d'Errico et al., 2022) and Tau (Wright, 2021), and produce pro-inflammatory cytokines such as interleukin IL-6 (Hickman et al., 2008). Low-grade neuroinflammation induced over decades, for instance by  $A\beta$  and free radical accumulation, chronic sleep deprivation, dysbiosis or vascular and metabolic disorders, can gradually cause damage to the blood-brain barrier (BBB) (Halliday et al., 2016; Nation et al., 2019; Noe et al., 2020). The alteration of the BBB integrity allows brain inflammatory mediators to reach the periphery, triggering peripheral innate and adaptive inflammatory responses (Le Page et al., 2018; Šimić et al., 2019). Conversely, metabolic disorders are well documented to trigger peripheral chronic oxidative stress and low-grade inflammation, which could increase the risk of developing AD and quadruple it in patients with mild cognitive impairment (Ng et al., 2016). For instance, IL-6 pathway in the brain has been identified as a potential link between cognitive impairment and peripheral metabolic alterations in AD (Lyra E Silva et al., 2021). Systemic inflammation and oxidative stress have been linked to the formation of  $A\beta$ , Tau phosphorylation and neuroinflammation, which in turn lead to an increased production of pro-inflammatory cytokines (Wang et al., 2018; Xie et al., 2021), and may serve as initiating factors in preclinical AD. Our laboratory and others have demonstrated that inflammatory and oxidative mediators can be disseminated through extracellular vesicles (EVs) (Haddad et al., 2021; Nielsen et al., 2021; Perrotte et al., 2020).

EVs are a variety of nanoscale membrane vesicles unable to replicate which are released by almost all cell types (van Niel et al., 2018). Among EVs, exosomes are a population characterized by a size inferior to 200 nm in diameter and a specific biogenesis pathway. Exosomes are formed intracellularly by endocytic invagination and generated by outward budding at the endosomal membrane of the multivesicular bodies. Given the lack of specific markers for EVs classification and recognition, the present study will employ the operational term EVs (Welsh et al., 2024). EVs are composed of a phospholipidic bilayer and cargo including lipids, proteins and RNAs which can be delivered to neighbouring or distant cells via different biofluids (van Niel et al., 2018). Therefore, EVs play an important role in cell-to-cell communication and regulation (van Niel et al., 2018). Once in the intercellular space, they can spread compounds to recipient cells. In the brain, exosomes as well as other small EVs (sEVs) have been demonstrated to transfer proapoptotic proteins, inflammatory factors, miRNAs promoting neuroinflammation (Ngolab et al., 2017) and neuronal damages (Pascual et al., 2020). They also participate in  $A\beta$  production and oligomerization (Perez-Gonzalez et al., 2012; Rajendran et al., 2006), disseminate  $A\beta$  (Ben Khedher et al., 2023) and Tau (Wang et al., 2017) to neighbouring neurons, which act as 'seeds' to amplify the toxic effects of misfolded proteins (Pascual et al., 2020). Additionally, sEV proteins seem to accumulate in the vicinity of  $A\beta$  plaques in AD brains (Rajendran et al., 2006). The injection of EVs released from HEK293-APP Swe/Ind cells into the dentate gyrus of mice has been demonstrated to impair adult hippocampal neurogenesis (Zheng et al., 2017). In contrast, the inhibition of exosome synthesis and release in the 5  $\times$  FAD mouse model has been shown to decrease the levels of  $A\beta_{1-42}$ , alleviate amyloid plaque load in the brain, and improve cognitive deficits (Dinkins et al., 2014, 2016). While sEVs are beneficial to the donor cells with the release of toxic compounds, they could be harmful to the recipient cells by propagating deleterious factors (Pascual et al., 2020; Sardar Sinha et al., 2018), thereby contributing to the development of AD (Counil & Krantic, 2020).

The role of EVs in AD pathogenesis may not be limited to a local influence at the cerebral level but could be part of a more complex and widespread action deriving from peripheral organs. For example, erythrocytes-derived EVs, containing large amounts of  $\alpha$ -synuclein, can cross the BBB and trigger  $\alpha$ -synuclein-related pathology (Matsumoto et al., 2017). We have recently demonstrated that, compared with plasma, plasma-derived EVs from AD patients can carry higher levels of  $A\beta$ , Tau, pro-inflammatory molecules and RAGE (Ben Khedher et al., 2021; Haddad et al., 2021; Perrotte et al., 2020). We also demonstrated that their levels can be used to discriminate disease stages (Haddad, Perrotte, Landri, et al., 2019). Although numerous studies have investigated the permeability of the BBB to peripheral EVs (pEVs) circulating in the blood, this question remains largely unsolved. Indeed, this permeability depends on several parameters, such as their specific molecular cargo and surface decoration by the protein coronae, which can modify the physiochemical properties of EVs. Likewise, the crossing of pEVs through the BBB has been shown to vary over 10-fold depending on their origins (Banks et al., 2020) and the level of BBB integrity. For instance, tumour-derived sEVs can translocate across the BBB by transcytosis (Morad et al., 2019), and EVs released from bone marrow (Ridder et al., 2014), cancer cells (Zhou et al., 2014) or activated monocytes (Saeedi et al., 2019) can alter the tight-junction proteins as well as the integrity of the endothelial cells or of the BBB. On the other hand, HEK293T cells-derived EVs can cross through the

brain microvascular endothelial cells (BMECs) monolayer only under stroke-like, inflamed condition (Chen et al., 2016). In some pathological conditions, EVs have been demonstrated to reach the brain, target cerebral cells (Ridder et al., 2014) and activate glial cells (Morales-Prieto et al., 2022). However, the crossing of pEVs through the BBB in a bidirectional manner to influence either cerebral or peripheral tissues remains obscure. Their ability to cross the brain barriers and their brain homing is one of the most outstanding unsolved issues and involve many concepts, including the implication of size diversity, biological effects, targeting and cell physiology.

In this regard, we hypothesized that pEVs derived from the serum of healthy adults, AD patients and age-matched control donors might exhibit different interactions with endothelial, neuronal and glial cells. The first objective of our study was to investigate whether fluorescently labelled pEVs cross differently the mouse bEnd.3 endothelial cells, used to model the BBB. The second objective was to examine the differential internalization by neuronal and microglial cells and their effect on microglia activity seeded at the bottom of the Transwell device. Finally, the passage of pEVs through the BBB was validated in vivo on 2-days post-fertilization (dpf) transgenic zebrafish *Danio rerio* Tg(*flkl:EGFP*) line expressing fluorescent-labelled endothelial cells, and their homing into specific brain cell lines was investigated with the Tg(*huc:EGFP*) and Tg(*gfap:EGFP*) lines, fluorescent-labelled neuronal and radial glial cells, respectively. Furthermore, these findings were validated in a mammalian model through the injection of pEVs into the mouse hippocampus. Our results highlight the significance of the communication axis from the periphery to the brain via the translocation of pEVs through the BBB, providing new insights on pEVs brain homing and raising new questions about the potential impact of pEVs in AD pathogenesis.

## 2 | MATERIALS AND METHODS

### 2.1 | Study design and participants

Healthy adult donors control (CTL), aged between 18 and 45 years old, without metabolic disorders or drug consumption for the last two weeks, were recruited at the Institut National de la Recherche Scientifique (INRS). Mild AD (mAD) patients and age-matched controls (healthy elderly controls, HeC) in the range of 66–88 years old were recruited from the registry of the memory clinic of the Geriatric Institute of Sherbrooke University. All protocols were approved by the Ethical Committees in Human Research (protocols #CER-20-582 for INRS, #2019-2877 for Sherbrooke University). Written informed consents were obtained from all participants before enrolment. Briefly, HeC patients have no history or overt physical signs of atherosclerosis or inflammation that satisfy the SENIEUR protocol criteria for immuno-gerontological research. The selection of mAD patients was based on criteria developed by the National Institute of Neurological and Communicative Disorders and Stroke and the Alzheimer's Disease and Related Disorders Association (NINCDS-ADRDA). The global cognitive function of mAD and HeC patients was evaluated by the Mini-Mental State Exam (MMSE) and the Montreal Cognitive Assessment (MoCA), and by an extensive neuropsychological examination. Atherosclerosis was assessed by electrocardiogram, carotid and lower leg ultrasound. Biochemical tests included renal and hepatic function, lipid status, blood cell count, albumin, thyroid hormones and cortisol, vitamin B12 and folate in erythrocytes. Blood was obtained after overnight fasting in dry tubes and centrifuged at 3000 rpm for 10 min at 4°C. Sera were stored at –80°C until analysis.

### 2.2 | Isolation, characterization, and labelling of pEVs

#### 2.2.1 | Isolation of pEVs

pEVs were extracted from the serum of CTL ( $n = 4$ ), HeC ( $n = 17$ ) and mAD ( $n = 17$ ) patients according to a protocol based on a precipitation method using the Total Exosome Isolation reagent (Invitrogen, MA, USA) with some modifications. Briefly, sera samples were clarified by centrifugation at  $10,000 \times g$  for 5 min to remove debris. The supernatant containing the clarified serum was used for EVs isolation. pEVs were precipitated with the Total Exosome Isolation reagent, then re-suspended and purified by a series of filtrations and precipitations as previously described (Ben Khedher et al., 2021). pEVs were characterized according to the Minimal Information for Studies of EVs criteria (Welsh et al., 2024).

#### 2.2.2 | Nanoparticle tracking analysis (NTA)

The concentration (particles/mL) and size distribution (nm) profile of pEVs were measured by NTA using a NanoSight NS300 instrument (Malvern Panalytica, UK). Videos were recorded at camera level 14 and the focus was manually adjusted. Each sample was diluted in pre-filtered MilliQ water and dilutions were adjusted to obtain particle concentration per frame between 40 and 90. For each sample, three videos of 60 s were recorded and analysed in batch-processing mode using the NTA 2.3 software (Malvern Panalytica, UK).

### 2.2.3 | Transmission electron microscopy (TEM)

TEM was used for the morphological examination of isolated pEVs. pEVs preparations were suspended in 2% paraformaldehyde (PFA). Ten microlitres of the mixture were loaded onto a Formvar-carbon coated grid for 5 min. Grids were negatively stained using 2% uranyl acetate solution for 1 min. The excess fluid was gently removed, and grids were observed using the HITACHI 7100 transmission electron microscope (75 kV, Japan) at 1500 $\times$ –40,000 $\times$  magnification, and images were captured using a digital camera (AMT XR111).

### 2.2.4 | Protein quantification

Proteins were extracted using radioimmunoprecipitation assay (RIPA) lysis buffer (50 mM Tris buffer, pH 8, 150 mM sodium chloride, 0.1% sodium dodecyl sulphate (SDS), 1% Igepal, 1% sodium deoxycholate, 5 mM EDTA, 1% protease and phosphatase inhibitors cocktail). The total protein concentration was determined by bicinchoninic acid assay (Pierce BCA Protein Assay Kit, ThermoFisher Scientific, MA, USA) at 562 nm using Synergy HT (BioTek Instruments, Inc., VT, USA).

### 2.2.5 | ELISA assay

The apolipoprotein A-I (ApoA1) levels were determined with a human ApoA1 DuoSet ELISA development kit (R&D Systems, MN, US) in a 96-well ELISA plate at 450 nm using a microplate reader (Synergy HT, Bio-Tek, VT, USA). ApoA1 levels were determined with an ApoA1 standard curve within the concentration range of 3.13–200 ng/mL and normalized to the total protein in the respective wells.

### 2.2.6 | Zeta potential

pEVs were suspended in 1 mL of PBS 1X (dilution 1:500, v/v) and placed in a disposable folded capillary cell on a Zetasizer Nano-ZS (Malvern Instruments, UK). Measurements were carried out in triplicate at 25°C.

### 2.2.7 | PKH26 labelling of pEVs

pEVs were labelled with the red fluorescent membrane dye PKH26 ( $\lambda_{\text{ex}}$  551 nm;  $\lambda_{\text{em}}$  567 nm; MIDI26, Sigma, MO, USA). Briefly, 100  $\mu$ L of fresh pEVs and the PKH26 dye were gently mixed in 250  $\mu$ L of dilution media for 10 min at room temperature. The reaction was stopped by adding 1/4 (v/v) of exosomes-depleted foetal bovine serum (Life Technologies Corporation, NY, USA) for 1 min. Excess of PKH26 was removed by washing in PBS 1X, filtered on a 100 kDa molecular weight filter (Millipore Sigma, MO, USA) and centrifuged at 3000  $\times$  g for 15 min at 4°C. The supernatants containing labelled pEVs were collected and kept overnight at 4°C before use. The analysis of PKH26-labelled pEVs was performed with the violet side scattering (V-SSC) using the 405 nm violet laser of the CytoFlex S (Beckman Coulter, CA, USA). The detection threshold for V-SSC was set at 1800 with a gain of 200. Samples were run with a slow flow rate (10  $\mu$ L/min) for 2 min until the event/second rate was stable and abort rates had decreased below 5%. The acquisition time was set at 30 s. Data were acquired and analysed using CytExpert 2.0 software (Beckman Coulter, CA, USA). Gated regions were determined to use unstained pEVs as controls. Relative diameters of pEVs were determined with standard submicron yellow-green, fluorescent polystyrene beads with 0.2 and 0.5  $\mu$ m sizes (Bangs Laboratories Inc. Fishers, IN, USA).

## 3 | CELL CULTURE

### 3.1 | Cell seeding in Transwells

For in vitro transcytosis experiments,  $2.5 \times 10^5$  bEnd.3 endothelial cells (ATCC CRL-2299TM, VA, USA) were seeded in a 6-well plate on the apical side of the Transwell insert with 1  $\mu$ m pore diameter and a surface area of 4.67 cm<sup>2</sup> (Corning Costar, MA, USA). The putative effect of FBS concentration (10% and 12%) on bEnd.3 cells permeability was assessed in a 24-well plate with Transwell insert with 1  $\mu$ m pore diameter and a surface area of 0.33 cm<sup>2</sup> (Corning Costar, MA, USA). Cells were maintained in a Dulbecco's Modified Eagle Medium (DMEM) containing FBS (either 10% v/v when incubated alone or with SK-N-SH cells,

or 12% v/v in the abluminal face when incubated with HMC3 cells), 1 mM sodium pyruvate, 100 U/mL penicillin, and 100 g/mL streptomycin in a humidified incubator at 37°C with 5% CO<sub>2</sub>. After confluence, bEnd.3 cells were allowed to build tight-junction proteins for at least 7 days (Koto et al., 2007). The bottom of the basal compartment was either seeded with 5 × 10<sup>5</sup> cells/well of SK-N-SH neuronal cells (ATCC HTB-11, VA, USA) or with HMC3 microglial cells (ATCC CRL-3304, VA, USA). Media volumes were either 1 mL in the apical and 2 mL in the basal compartments for the 6-well plate device, or 0.5 mL in the apical and 1 mL in the basal compartments for the 24-well plate device. Media were changed every other day for 7–10 days of culture.

## 3.2 | Permeability assays

### 3.2.1 | TEER measurement

The transepithelial/transendothelial electrical resistance (TEER) is the electrical resistance across a cellular monolayer and represents a very sensitive and reliable index to confirm the integrity of the monolayer. The TEER was measured using the epithelial voltohmmetre metre equipped with an STX2 electrode set for EVOM2 (World Precision Instruments Inc., FL, USA). The background value measured on the cell-free inserts was subtracted from the total TEER measurement. The calculation of resistivity ( $\Omega \text{ cm}^2$ ) was as follows:

$$TEER = (\text{Resistance } (\Omega) - \text{Insert Resistance } (\Omega)) \times \text{Surface area } (\text{cm}^2)$$

### 3.2.2 | Dextran FITC

The integrity of the cell monolayer was also assessed 10 days after seeding with the permeability of the Dextran-FITC (10 kDa, Sigma-Aldrich, MO, USA) as described previously (Rabanel et al., 2020). Briefly, 10  $\mu\text{L}$  of a 1 mg/mL solution of 10 kDa Dextran-FITC was added in a serum-free media without phenol to the apical side of the insert. After 1-h of incubation at 37°C, 150  $\mu\text{L}$  of the basal and the apical compartments was collected and analysed in a fluorescent microplate reader, at  $\lambda_{\text{ex}}$  485 and  $\lambda_{\text{em}}$  525 nm (SpectraMax Plus 384 Microplate Spectrophotometer, Molecular Devices LLC, CA, USA). The apparent permeability index ( $P_{\text{app}}$ ) was calculated as the following equation:

$$P_{\text{app}} = \frac{V_R \Delta C_R}{\Delta t S_{\text{ins}} C_D}$$

with  $P_{\text{app}}$  apparent permeability (cm/s);  $V_R$ , volume of the apical side (cm<sup>3</sup>),  $\Delta C_R$ , change in concentration in the basal receiving compartment ( $\mu\text{M}$ );  $\Delta t$ , time in seconds (s);  $S_{\text{ins}}$ , surface of the insert (cm<sup>2</sup>); and  $C_D$ , concentration in the apical compartment ( $\mu\text{M}$ ).

## 3.3 | Western blotting

20  $\mu\text{g}$  of total protein samples were heated for 5 min at 95°C in a denaturing buffer containing  $\beta$ -mercaptoethanol and SDS. Samples were then loaded on a 10% of polyacrylamide gel electrophoresis then transferred to a polyvinylidene difluoride (PVDF) membrane using the Trans Blot Turbo Biorad system. Then membranes were incubated with 5% skim milk in TBS-T (Tris-buffered saline Tween) blocking solution for 1-h at room temperature under shaking. Next, membranes were incubated overnight at 4°C with primary antibodies. To study the expression of tight-junction proteins by bEnd.3 cells, we used the primary antibodies anti-mouse ZO-1 (1:100, Invitrogen, MA, USA) or anti-rabbit Claudin-5 (1:500, Invitrogen, MA, USA). For pEVs proteins, membranes were incubated with the primary antibodies TSG101 (1:2500, MyBioSource, CA, USA), CD63 (1:500, Santa Cruz, CA, USA), ALIX (1:500, Covalab, France), or calnexin (1:500, Santa Cruz, CA, USA). Membranes were then washed three times for 10 min with TBS-Tween 0,1% at room temperature and incubated with the secondary antibodies labelled with HRP anti-rabbit antibodies (1:5000, Cell Signaling Technology, MA, USA) or HRP anti-mouse antibody (1:1000, Cell Signaling Technology, MA, USA) for 1-h at room temperature under shaking. After three washes in TBS-Tween 0,1%, proteins were detected by chemiluminescence using the ECL substrate and the ChemiDoc XRS + system (Bio-Rad Laboratories, Canada). Total proteins on the membranes were stained with Coomassie blue.

### 3.4 | pEVs endocytosis and uptake by bEnd.3, SK-N-SH and HMC3 cells

#### 3.4.1 | Endocytosis analysis by flow cytometry assay

The endocytosis analysis of pEVs was carried out in a 6-well plate with the Transwell devices (1  $\mu\text{m}$  pores, Corning Costar, Cambridge, MA), with or without SK-N-SH or HMC3 cells seeded at the bottom. After confluence and establishment of the integrity of the bEnd.3 cells monolayer,  $1 \times 10^{10}$  pEVs/mL were added to the 1 mL of apical medium without Phenol Red. After 24 h, bEnd.3 cells monolayer, SK-N-SH or HMC3 cells were washed twice with cold PBS. After trypsinization (Trypsin/EDTA 0.25%) at 37°C for 5 min, the cell suspensions were transferred to 5 mL tubes (Falcon, Corning, NY, USA) and centrifuged at 4000 rpm for 4 min (Sorvall Legend RT+, ThermoFisher Scientific, MA, USA). Cells were then washed with PBS at pH 7.4, and finally resuspended in 0.5% PFA/PBS. Internalization of PKH26-labelled pEVs was analysed on the BD Fortessa cytometer (Becton-Dickinson, MA, USA) using Diva software (Becton Dickinson, MA, USA) with the PE channel ( $\lambda_{\text{ex}}$  551,  $\lambda_{\text{em}}$  567 nm).

#### 3.4.2 | Endocytosis analysis by immunochemistry assays

The internalization of pEVs by different cell types was confirmed by immunochemistry after 24 h. bEnd.3 and either SK-N-SH or HMC3 cells were, respectively, seeded on the Transwell device and on pretreated glass slide until confluence. Briefly, 24 h after the incubation with PKH26-labelled pEVs, cells were fixed with 4% PFA/PBS, then permeabilized with 0.25% vol/vol of Triton X100 in PBS containing  $\text{Ca}^{2+}/\text{Mg}^{2+}$  (PBS- $\text{Ca}^{2+}/\text{Mg}^{2+}$ ) for 10 min. After three washings with PBS- $\text{Ca}^{2+}/\text{Mg}^{2+}$ , cells were incubated for 1-h in a blocking solution composed of 0.25% Tween 20 in PBS (PBS-T)/5% BSA (vol/vol). Then bEnd.3 cells were incubated for 2 h at room temperature under shaking with the primary antibodies anti-mouse ZO-1 (1:200, Invitrogen, MA, USA) or anti-rabbit Claudin-5 (1:200, Invitrogen, MA, USA) while the SK-N-SH and the HMC3 cells were, respectively, incubated with the primary antibody anti-mouse  $\beta$ -III Tubulin (1:200, Sigma-Aldrich, MO, USA) and anti-rabbit Iba1 (1:500, Abcam, UK), followed by the secondary antibodies anti-mouse CY5 (1:500, Invitrogen, MA, USA) or anti-rabbit Alexa fluor 488 (1:500, Invitrogen, MA, USA) for 1-h. After three washings with PBS- $\text{Ca}^{2+}/\text{Mg}^{2+}$ , the nuclei were counter stained with Hoechst 33342 for 10 min (1:10,000, Invitrogen, MA, USA). After additional washings, cells were mounted on a glass slide using Prolong Antifade mounting medium (ThermoFisher Scientific, MA, USA). Image analysis was performed in 3D using a Zeiss LSM780 multiphoton/confocal microscope (Zeiss, Germany). All the images were analysed with Zen 2.6 software (blue and black editions, Zeiss, Germany).

#### 3.4.3 | Live imaging

HMC3 cells were seeded on the 35 mm glass bottom dishes ( $\lambda$ -Irradiated, MatTek Corporation, MA, USA) at the density of 500,000 cells/mL in EMEM 12% with FBS for 24 h. Prior recording, the media was changed for EMEM without Phenol Red and FBS. After a few minutes of live recording,  $1 \times 10^{10}$  PKH-pEVs/mL from different groups of patients were added and the uptake was recorded for 3 h. 100  $\mu\text{L}$  of WGA-Alexa 680 conjugated (0.1 mg/mL, W21404, Invitrogen, MA, USA) were added at the end to visualize cell membranes.

### 3.5 | Toxicity assay

The putative cytotoxic effect of pEVs was assessed on bEnd.3, SK-N-SH and HMC3 cells. Briefly,  $2 \times 10^4$  cells per well were seeded in 96-well plates (Corning Incorporated, NY, USA) and incubated for 24 h in a humidified incubator at 37°C with 5%  $\text{CO}_2$ . Then the media was changed for a new one without Phenol Red and FBS, and cells were treated with either PBS,  $\text{H}_2\text{O}_2$  (1 mM), or different concentrations of fresh pEVs. Cells survival was assessed 24 h after using the Tox-8 Resazurin-based kit (Sigma-Aldrich, MO, USA) following the manufacturer's instructions and was determined by spectrophotometry at  $\lambda_{\text{ex}}$  530 and  $\lambda_{\text{em}}$  590 nm (Synergy HT plate reader, BioTek Instruments, Inc., Winooski, VT, USA). Cell viability percentage was calculated according to the PBS-treated condition.

### 3.6 | ELISA assay for IL-6 release by HMC3 cells

HMC3 cells were seeded in 96-well plates (Corning Incorporated, NY, USA) at the density of  $2 \times 10^4$  cells per well and incubated for 24 h in a humidified incubator at 37°C with 5%  $\text{CO}_2$ . Then media was changed for a new one without Phenol red and FBS, and cells were treated with either 1  $\mu\text{M}$  of human  $\text{A}\beta_{1-42}$  oligomers (oA $\beta_{1-42}$ , LifeTein, NJ, US) prepared according to Stine and colleagues (Stine et al., 2011), 1  $\mu\text{g}/\text{mL}$  lipopolysaccharide (LPS L3129, Sigma-Aldrich, MO, USA) or  $1 \times 10^{10}$  pEVs/mL from CTL,

HeC or mAD patients for 24 h. The levels of IL-6 released in the incubation medium were determined by the DuoSet ELISA (human IL-6 specific, R&D Systems, MN, US), according to the manufacturer's instructions. Briefly, aliquots of 100  $\mu$ L of pure incubation medium from control groups and 100  $\mu$ L of incubation medium diluted at 1:10 from the treated medium were dosed by ELISA. A standard curve was generated within the concentration range of 9.38–600 pg/mL and the optical density was quantified using a microplate reader (Synergy HT, Bio-Tek, VT, USA) set to 450 nm.

## 4 | IN VIVO DISTRIBUTION AND BRAIN HOMING OF pEVs IN ZEBRAFISH LARVAE

### 4.1 | Zebrafish models

Wild-type (WT) *Danio rerio*, also known as Tupfel long-fin (TL) strain, *Tg(flk1:EGFP)* expressing eGFP, an enhanced green fluorescence protein under the control of *kdrl* promoter regulating the expression of vascular endothelial growth factor receptor 2 (VEGFR-2) in vascular endothelial cells (Jin et al., 2005), *Tg(huc:EGFP)* expressing eGFP in mature neuronal cells (Park et al., 2000) and *Tg(gfap:EGFP)* expressing eGFP in an glial-like population (Raponi et al., 2007) zebrafish were used for these experiments. The zebrafish were maintained at 28°C and kept under a 12/12 h light/dark cycles at the animal facility of the Laboratoire National de Biologie Expérimentale (LNBE, Laval, Canada). They were bred according to standard procedure and staged as previously described (Kimmel et al., 1995). All experiments were performed in compliance with the guidelines of the Canadian Council for Animal Care and the local ethics committee.

### 4.2 | Intravascular injection of PKH-pEVs

For imaging studies, pigment formation was blocked by adding 0.003% phenylthiourea (PTU) dissolved in egg water at 24 h post-fertilization (hpf). Some larvae were incubated with Hoechst 33342 (30 ng/mL, Invitrogen, MA, USA) overnight for nucleus labelling prior to the injection. For the intravascular injection of PKH-pEVs, 48 hpf larvae were anesthetized with a tricaine Methanesulphonate (MS-222) solution (100 mg/L), then immobilized on the side in 1.5% low melting point agarose (UltraPure LMP Agarose, Invitrogen, MA, USA) with 0.0168% of tricaine, in 35 mm Glass bottom Petri dishes (MatTek Corporation, MA, USA). Zebrafish larvae were injected in the duct of Cuvier using a micropipette (Borosilicate Glass Micropipette with filament, 1.0 mm OD, 0.75 mm ID, 10 cm length, Sutter Instrument, USA) pulled on a Flaming/Brown Micropipette Puller Model P97 (single-line program with heat 340, filament 4, velocity 32, and delay 200, Sutter Instrument, USA). Volumes of injection were controlled by the measurement of droplet size in mineral oil. The total blood volume of zebrafish at 2 dpf has been estimated to be 60 nL (Craig et al., 2012), so the blood volume is not altered upon injection of 4.5 nL. The positioning of the micropipette was controlled with a manual micro-manipulator MN-153 (Narishige, Zeiss Canada Ltd., Canada). The injection pressure, volume and length were controlled with a nanoinjector FemtoJet 4i (Eppendorf, Germany). After injection, larvae were maintained at 28°C and only those maintaining robust heartbeat were selected. The BBB integrity at 2 and 3 dpf was confirmed by injection of either 10 kDa Rhodamine B-Dextran or 2 MDa FITC-Dextran. Confocal imaging was performed on a LSM780 confocal microscope (Leica, Germany) using 10 $\times$ , 20 $\times$  and 40 $\times$  objectives. Images were analysed using Zen 2.6 Blue and Black (Zeiss, Germany), and Imaris software (Oxford Instruments, UK).

### 4.3 | Pharmacological inhibition of exosomes release

To confirm that the signal related to PKH-pEVs originated from the exogenous injected EVs and not from newly formed endogenous vesicles, a pharmacological inhibition of exosome release was induced on some zebrafish larvae. In this regard, we used Manumycin A, an inhibitor of Ras farnesyltransferases involved in exosomes release, and GW4869, an inhibitor of membrane neutral sphingomyelinase, involved in exosome biogenesis. Zebrafish larvae were treated with either DMSO (0.5%) or Manumycin A (200  $\mu$ g/mL) combined with GW4869 (4  $\mu$ g/mL) in DMSO (0.5%) for 2 h at 28°C, then PKH-pEVs were intravenously injected.

## 5 | STEREOTAXIC INJECTION OF pEVs AND THEIR IN VIVO DIFFUSION IN THE MOUSE BRAIN

WT C57BL/6J mouse strain was purchased from the Jackson Laboratory (JAX, ME, USA). Mice were housed at the animal facility of the LNBE (Laval, Canada) with littermates and free access to food and water under a 12-h light/day cycle. Animal procedures were performed under the guidelines of the Canadian Council for Animal Care and the local ethics committee.

A total of  $2 \times 10^9$  PKH-pEVs from CTL patients or 3  $\mu\text{L}$  of PBS were stereotaxically injected in the CA1 area of the hippocampus of 12-month-old mice, using the following coordinates: anteroposterior  $-2.00$  mm; mediolateral  $\pm 1.8$  mm; dorsoventral  $-1.5$  mm. Mice were sacrificed 30 min or 1-h post-injection, and intracardially perfused with PBS followed by 4% PFA. Brains were removed and fixed in 4% PFA at  $4^\circ\text{C}$  for 24 h, followed by immersion in 15% sucrose for 12 h, and finally in 30% sucrose until total immersion. Brains were snap-frozen with isopentane and conserved at  $-80^\circ\text{C}$ . For immunohistological staining, coronal brain cryostat sections ( $20 \mu\text{m}$ ) were first washed 3 times with PBS- $\text{Ca}^{2+}/\text{Mg}^{2+}$ , and blocked for 1-h with a solution of PBS, 5% BSA, 0.25% Tween-10 at room temperature. Brain slices were incubated with the primary antibodies anti-rabbit GFAP (1:1,000, Sigma-Aldrich, MO, USA) and anti-mouse Neun (1:1000, Chemicon International, CA, USA) overnight at  $4^\circ\text{C}$ . Then, the slices were incubated for 2 h with the secondary antibodies anti-rabbit Alexa Fluor 488 (1:2000, Invitrogen, MA, USA) and anti-mouse CY5 (1:1000, Invitrogen, MA, USA). The nuclei were counter-stained with Hoechst 33342 for 10 min (1:10,000, Invitrogen, MA, USA). The brain slices were finally mounted on a glass slide using Prolong Antifade mounting medium (ThermoFisher Scientific, MA, USA). Image analysis was performed in 3D using a Zeiss LSM780 multiphoton/confocal microscope (Zeiss, Germany). All the images were analysed with Zen 2.6 software (blue and black editions, Zeiss, Germany).

## 6 | STATISTICAL ANALYSIS

Data are presented as mean  $\pm$  SEM and the normality of each distribution was evaluated prior statistical analysis. All comparisons between two groups used a student's *t*-test for paired samples unless otherwise noted with Prism 10 (GraphPad Software Inc, USA). One-way analysis of variance was used for experiments with three or more comparison groups. For significant differences, *p*-values were presented such as  $*p \leq 0.5$ ;  $**p \leq 0.05$ ;  $***p \leq 0.005$ ;  $****p \leq 0.0005$ .

## 7 | RESULTS

### 7.1 | pEVs isolation and characterization from human subjects

All groups included individuals of both sexes. Demographic, clinical and biochemical (blood cholesterol and glucose levels) data from HeC and mAD patients are shown in Figure S1. CTL subjects were significantly younger than the other two groups, free of any metabolic disease, and cognitively normal. MMSE and MoCa scores were significantly lower in mAD as compared to HeC. Total cholesterol levels were significantly higher in mAD than in HeC, whereas glucose levels were similar in both groups.

The TEM images pointed to cup-shaped morphology reminiscent of the presence of a lipid-rich layer compatible with EVs morphological features with a size below 200 nm, which could correspond to exosomes (Figure 1a). More detailed NTA analysis revealed that the size of EVs ranged from 50 to 300 nm (Figure 1b). The size distribution of pEVs was similar between CTL and HeC, but their number decreased with age for the vesicles comprised between 100 and 300 nm (Figure 1c). Interestingly, the pEVs number and size varied with the age and health status, especially for pEVs between 50 and 150 nm in diameter (Figures 1c,f). Remarkably, in the mAD group the size distribution analysis pointed to higher numbers of pEVs between 50 and 150 nm (1.9-fold more than CTL and 4.5-fold more than HeC) (Figures 1d,e,f). Conversely, the number of pEVs greater than 150 or 200 nm was lower in mAD compared to HeC or CTL.

The total pEVs protein is similar in all three groups (Figure 1g). Proteins involved in exosome biogenesis such as ALIX, TSG101 and CD63 were highly expressed in pEVs, whereas Calnexin, the negative control, was expressed only in SK-N-SH neuroblastoma lysate and human CTL serum, thus attesting pEVs enrichment (Figure 1h). Contamination of albumin (Figure 1i) and ApoA1 ( $10.39\text{--}13.77$  ng/mL for pEVs vs.  $4.5 \times 10^4$ – $5.4 \times 10^4$  ng/mL for sera) was minor (Figure 1j). The zeta potential of the pEVs from CTL was on average  $-19.42$  mV, indicating an anionic state in the optimal range and suggesting that the enrichment procedure did not alter their property. Of note, with increasing age, the zeta potential was less negative and was significantly lower in HeC than in CTL (Figure 1k). However, pEVs HeC presented a more positive charge on their surface ( $-11.95$  mV) than pEVs mAD ( $-15.03$  mV). This difference in the zeta potential did not affect the percentage of labelling of pEVs (23.41%) with the PKH-26 probe (Figures 1l,m). As pEVs were isolated from human serum, genetic labelling was not possible. Given that PKH is a transmembrane dye offering a strong signal, we used PKH26 to conduct our in vitro and in vivo experiments. To confirm the efficacy of labelling, PKH-pEVs were subjected to degradation with Triton X100, which induces the loss of the PKH-pEVs signal and validates the absence of free PKH. Only samples without contamination of free PKH were used for in vitro and in vivo experiments (Figure 1m).



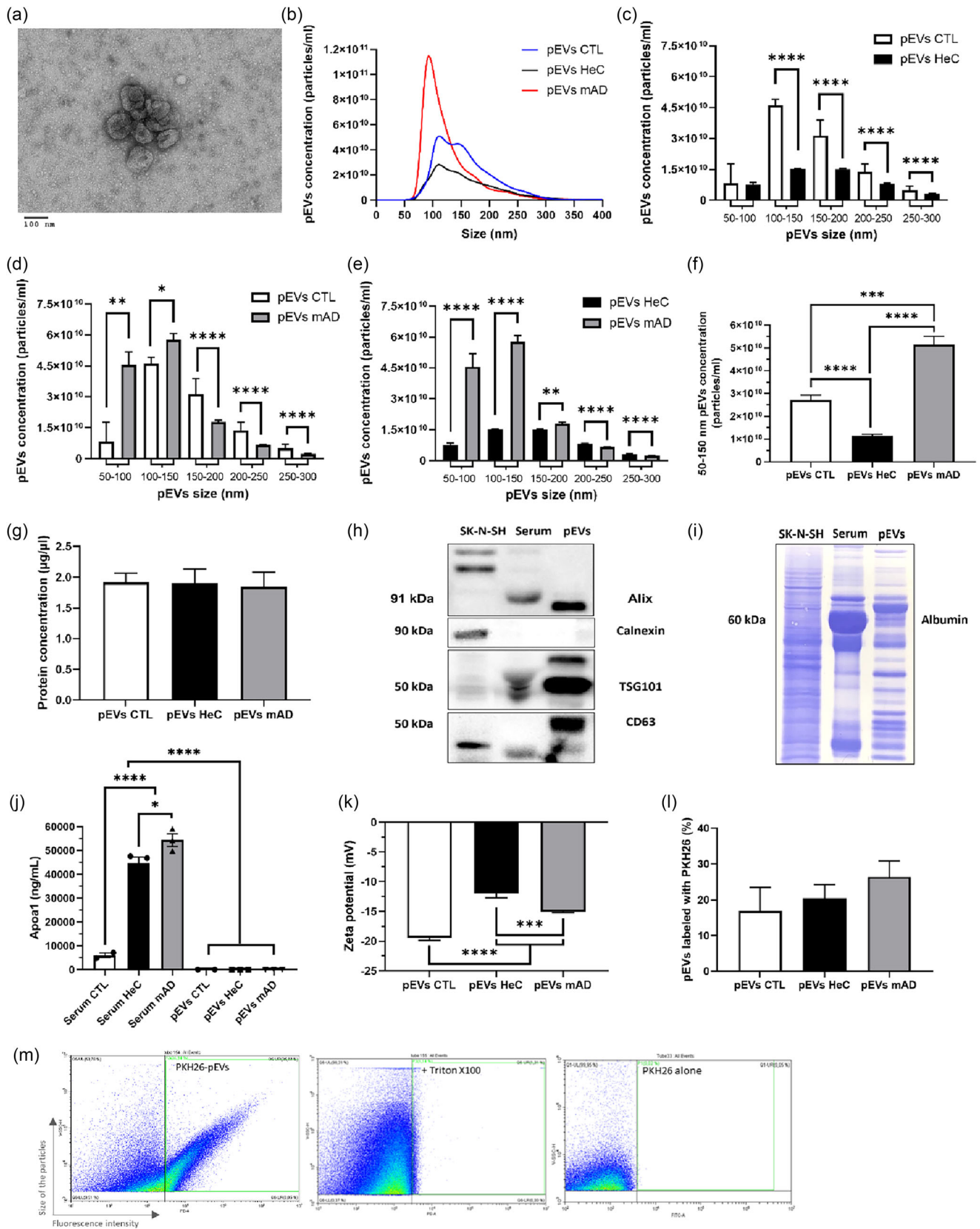


**FIGURE 1** Characterization of pEVs isolated from human sera. (a) TEM images. (b)–(f) NTA analysis and concentrations of pEVs stratified by size range in CTL ( $n = 4$ ), HeC and mAD patients ( $n = 17$  per group). Differences were analysed by the Mann–Whitney test. (g) Protein concentrations in pEVs were compared by ordinary one-way ANOVA followed by Tukey’s multiple comparisons test. (h) Immunodetection of EVs markers Alix, TGI01, CD63. Calnexin was used as a negative control. (i) Total proteins remaining on PVDF membrane after the transfer revealed by Coomassie blue. (j) Levels of ApoA1 in the sera

(Continues)

**FIGURE 1** (Continued)

and pEVs were compared by ELISA and compared by ordinary one-way ANOVA followed by Tukey's multiple comparisons test. (k) Zeta potential was determined by DLS and compared by ordinary one-way ANOVA followed by Tukey's multiple comparisons test. (l) Comparison of the percentage of pEVs labelled with the fluorescent dye PKH-26, by unpaired *t*-test. (m) Nanoscale flow cytometry analysis of the pEVs labelled with the fluorescent dye PKH-26, with and without the addition of 0.2% Triton X100, and analysis of free PKH26 without pEVs. All samples were diluted at 1:1000. Prior statistical analysis, the normality of each data set was evaluated. Data are expressed as mean  $\pm$  SEM with \* $p \leq 0.5$ ; \*\* $p \leq 0.05$ ; \*\*\* $p \leq 0.005$ ; \*\*\*\* $p \leq 0.0005$ . pEVs, peripheral EVs; TEM, transmission electron microscopy.

## 7.2 | pEVs pass through endothelial cell monolayer and are internalized by neuronal and microglial cells

Before assessing the ability of pEVs to cross the endothelial cell monolayer and their subsequent internalization by neuronal or microglial cells, we first evaluated the potential toxicity of pEVs to bEnd.3, SK-N-SH and HMC3 cells. No toxic effect on any of the three cell types was observed up to the highest concentration tested ( $1 \times 10^6$  pEVs/cell) (Figure S2). In additional preliminary experiments, we further verified the establishment of tight-junction proteins between bEnd.3 cells forming the monolayer after seeding on the Transwell device with either neuronal or microglial cells seeded at the bottom of the device (Figure S3a). Measuring the TEER of bEnd.3 cells monolayer every other day, with either SK-N-SH or HMC3 cells seeded at the bottom, indicated that a plateau was reached after 6 days (265  $\Omega$  cm, Figure S3b). The integrity of bEnd.3 cells monolayer was assessed at Day 10 by measuring the apparent permeability ( $P_{app}$ ), which is based on the flux of 10 kDa Dextran FITC across the cell monolayer for 1-h. For the bEnd.3 cells monolayer cultured with SK-N-SH or HMC3 cells, the  $P_{app}$  was, respectively, between 0.006 and 0.009 cm/s, which is 2.98 times and 2.45 times less than in the absence of the monolayer (0.018 to 0.023 cm/s, Figure S3c). The observed  $P_{app}$  was in the same range as previously published data using the same model (Li et al., 2010; Rabanel et al., 2020). As bEnd.3 cells were cultured with 10% (SK-N-SH) or 12% (HMC3) of FBS, we tested the impact of the percentage of FBS on the  $P_{app}$ . Our data showed that  $P_{app}$  was not different with 10% or 12% of FBS (Figure S3d). Finally, the expression and localization of ZO-1 and Claudin-5 were confirmed on the Transwell by immunohistochemistry and by Western blotting from cells cultured in T75 flasks (Figures S3e,f).

The passage of pEVs through the bEnd.3 was first assessed with SK-N-SH cells seeded at the bottom (Figure 2). After 10 days of culture,  $1 \times 10^{10}$  pEVs/mL derived from either CTL, HeC or mAD patients were added to the luminal compartment for 24 h. The pEVs did not change the permeability of bEnd.3 monolayer as shown by the  $P_{app}$  assay (Figure 2b). However, after 24 h of treatment, we found that the TEER was reduced by  $-42.86\%$  in the presence of pEVs derived from mAD patients as compared to pEVs obtained from CTL and HeC patients, or PBS condition (Figure 2c). These results suggest an alteration of the bEnd.3 monolayer by pEVs from mAD patients. We have then explored its integrity by assessing the expression of tight-junction proteins by IHC 24 h after the treatment. IHC data pointed to a fully preserved integrity of the monolayer (Figure 2d). The interaction of PKH-pEVs with the cell surface of bEnd.3 monolayer and their cellular uptake were analysed by IHC and confocal imaging (Figure 2e). Twenty-four hours after the addition of pEVs in the luminal medium, flow cytometry demonstrated that PKH-pEVs were internalized by bEnd.3 cells (in 62.61% to 68.76% of the cells). However, there was no differential uptake between the three groups of pEVs (Figures 2f,g). Interestingly, PKH-pEVs were found in the perinuclear area of the bEnd.3 cells. The presence of PKH-pEVs into the luminal and abluminal media was confirmed by nanoflow cytometry, demonstrating that pEVs passed through the bEnd.3 cells monolayer (Figure 2h). PKH-pEVs were mostly detected in the luminal face and to a lower extent in the abluminal face.

Subsequently, the interaction of PKH-pEVs with SK-N-SH cells was studied by IHC and confocal imaging. pEVs were placed either directly with neuronal cells (Figure 3a) or in the luminal chamber with the bEnd.3 cells monolayer on the Transwell device (Figure 3b). The background related to PKH-pEVs was obtained with PBS treatment (Figure 3c). We first ascertained that PKH-pEVs interacted with the cellular surface of SK-N-SH cells, with or without the monolayer (Figures 3d,e). PKH-pEVs were observed on the axons but were seen more abundantly on SK-N-SH cell bodies. However, the signal related to internalized PKH-pEVs was lower when the neuronal cells were cultured with bEnd.3 cells, indicating that the endothelial monolayer retained a certain amount of pEVs. The quantification of the internalization of pEVs by SK-N-SH cells seeded at the abluminal compartment was carried on by flow cytometry (Figures 3f,g). The engulfment of pEVs by SK-N-SH cells was high following a direct treatment (i.e., 51.03% of SK-N-SH cells were fluorescent), lower in the presence of the Transwell device (14.07% without cell monolayer) and even lower (5.07%) in the presence of the bEnd.3 cells monolayer. These results indicate that at least 5% of SK-N-SH cells have engulfed PKH-pEVs released by the bEnd.3 cells (Figure 3g).

We next studied the passage of pEVs through the bEnd.3 cells monolayer in the presence of microglial HMC3 cells (Figure 4a). The internalization of PKH-pEVs by bEnd.3 cells and the expression of the tight-junction proteins Clau-5 and ZO-1 were confirmed by IHC (Figure 4b). After 24 h of treatment with  $1 \times 10^{10}$  pEVs/mL extracted from CTL, HeC or mAD patients, PKH-pEVs were taken up by bEnd.3 cells and were mostly located in the perinuclear area similar to the localization observed in neuronal cells. Interestingly, by flow cytometry we observed that in the presence of HMC3 cells, the uptake of PKH-pEVs derived from

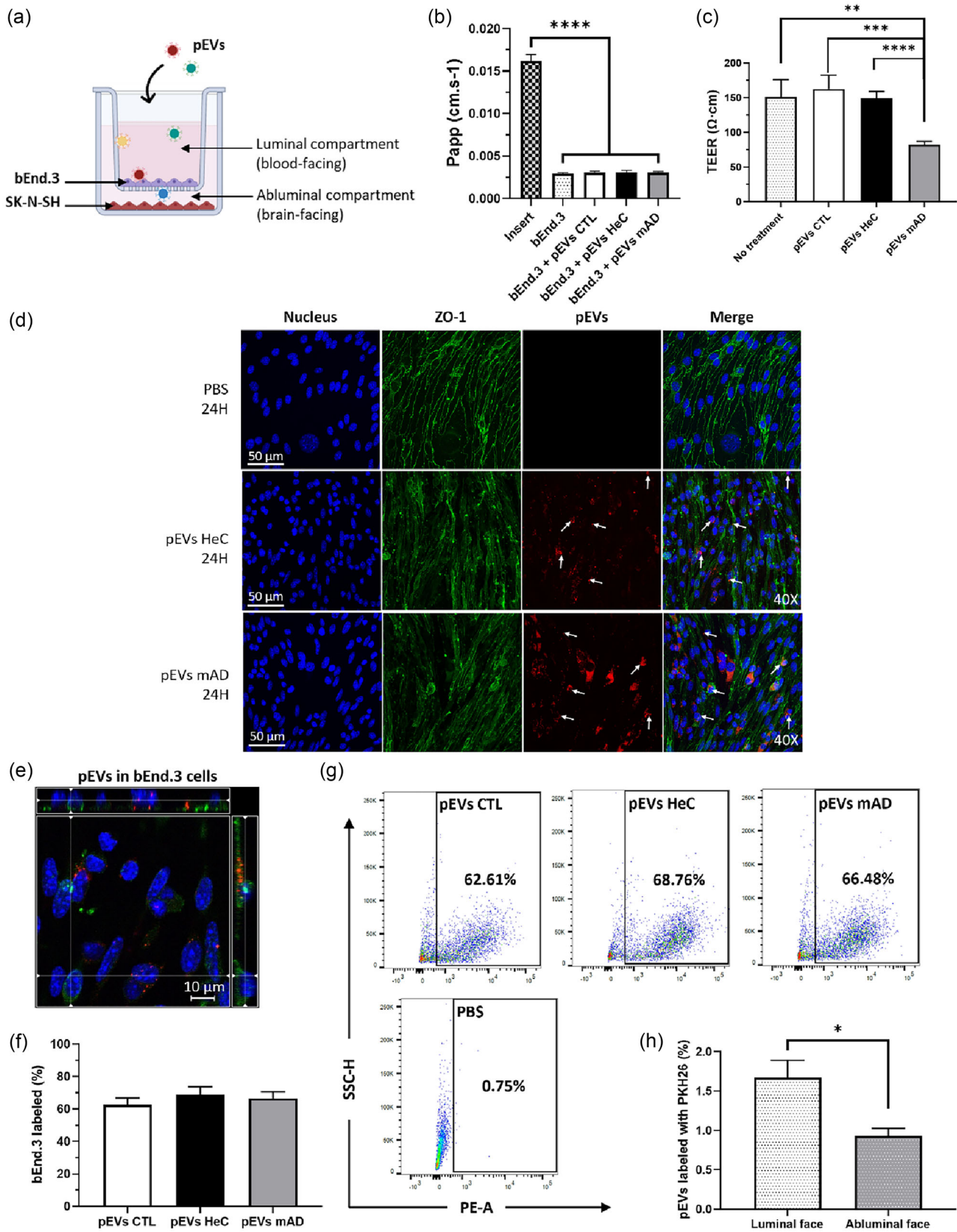


**FIGURE 2** Passage of pEVs through bEnd.3 endothelial cells in the presence of SK-N-SH neuronal cells. (a) bEnd.3 cells were cultured on a Transwell for 10 days with SK-N-SH cells seeded at the bottom, then  $1 \times 10^{10}$  pEVs/mL were added at the luminal side for 24 h. (b)  $P_{app}$  of bEnd.3 cells untreated and treated with pEVs were compared by ordinary one-way ANOVA. (c) Measurement of the TEER after 24 h of treatment with either PBS or pEVs. Groups were compared by the Kruskal–Wallis test. (d) Confocal imaging of pEVs (in red, indicated by arrows) internalized by bEnd.3 cells (nucleus in blue, ZO-1 in green).

(Continues)

**FIGURE 2** (Continued)

(e) Internalization of PKH-pEVs (in red, indicated by arrows) by bEnd.3 cells (nucleus in blue, ZO-1 in green) with their nucleus labelled (in blue) (40 $\times$ ). (f)–(g) Percentage of bEnd.3 cells internalizing the PKH-pEVs from different groups were quantified by flow cytometry and compared by ordinary one-way ANOVA. (h) The percentage of PKH-pEVs in the luminal and abluminal media was assessed by nanoscale flow cytometry and compared by the Wilcoxon matched-pairs signed rank test. Prior statistical analysis, the normality of each data set was evaluated. Data are expressed in mean  $\pm$  SEM with \* $p \leq 0.05$ ; \*\* $p \leq 0.005$ ; \*\*\* $p \leq 0.0005$  with  $n \geq 6$  per group. pEVs, peripheral EVs.

HeC and mAD patients by bEnd.3 cells was higher (respectively 95.78% and 94.40% of fluorescent cells) compared to the pEVs extracted from the CTL group (91.03%) (Figures 4c,d).

Direct treatment of HMC3 cells with  $1 \times 10^{10}$  pEVs/mL from CTL patients at 4 $^{\circ}$ C showed an absence of fluorescence after 1-h, which confirmed an energy-dependent uptake mechanism (Figure 5c). Interestingly, when HMC3 cells were incubated with PKH-pEVs for 1-h at 37.5 $^{\circ}$ C, the brightness and the density of the signal were similar to those observed after 24 h of treatment with SK-N-SH cells (Figures 3d,c). Notably, after 24 h, the signal intensity of PKH-pEVs in HMC3 cells was significantly lower than the 1-h mark and lower than the intensity observed in bEnd.3 or SK-N-SH cells at 24 h. One-hour post-treatment, HMC3 cells displayed a round shape and were close to each other. However, after 24 h they switched toward an active state and exhibited an elongated and more complex morphology. PKH-pEVs were observed mostly close to the cellular bodies and on microglial ramifications.

When HMC3 cells were cultured with bEnd.3 cells monolayer on the Transwell device, 24 h after adding PKH-pEVs from HeC or mAD patients to the luminal compartment, the uptake of PKH-pEVs by HMC3 cells was lower than with a direct treatment without the Transwell device (Figure 5d). Moreover, after 24 h, the intensity of the fluorescence was low, suggesting a degradation of the pEVs and/or the release of free PKH26 probe by the microglial cells. Interestingly, cells move toward the fluorescent signal, probably to engulf the PKH-pEVs in the abluminal side (Figure 5d), and their morphology switches from ramified to amoeboid (Figure 5d). PKH-pEVs were observed at the surface and inside HMC3 cells (Figure 5e).

The interactions between pEVs mAD and HMC3 cells were recorded by live imaging at 37.5 $^{\circ}$ C (Figure S4). The recording started a few seconds after the addition of PKH-pEVs mAD ( $1 \times 10^{10}$  pEVs/mL, Figure S4a) and lasted for 3 h. The video demonstrated that while some pEVs remained circulating in the media, others interacted with the cells within a few minutes (Figure S4b). Most of the interactions occurred in the cell body. Additionally, a portion of the pEVs was observed on or within the microglial branches connecting two cells, indicating that pEVs may be transported between microglial cells by direct contact. After 3 h, we added WGA Alexa 680-conjugated to label the cell membranes (Figure S4c) and found that most of the PKH-pEVs were internalized by the HMC3 cells. The presence of orange dots confirmed the interaction of some PKH-pEVs with the membrane of HMC3 cells (Figures S4d,e).

Subsequently, the engulfment of PKH-pEVs from CTL, HeC or mAD patients by HMC3 cells was quantified using flow cytometry (Figures 5f,g). After 24 h of exposure to PKH-pEVs CTL, the percentage of fluorescent microglial cells was, respectively, 95.20% and 76.30% without and with the Transwell device, indicating that the passive diffusion through the Transwell device represents around 19% (Figure 5g). The percentage of HMC3 cells internalizing PKH-pEVs was normalized according to the HMC3 cells with pEVs CTL and insert condition. Hence, compared to a direct treatment (95.2% for pEVs CTL), a significant decrease in the number of fluorescent HMC3 cells was observed in the presence of the Transwell (76.30% for pEVs CTL) or with bEnd.3 monolayer (1.28% for pEVs CTL), demonstrating a retention of the PKH-pEVs by the filter and the endothelial cells (Figure 5g). Interestingly, the internalization by HMC3 cells is higher for pEVs derived from HeC (5.12%) and mAD patients (7.11%) as compared to pEVs CTL (1.28%).

To gain further insight into the differential effect of the pEVs on the activity of the microglial, the release of IL-6 was analysed according to their origins (CTL, HeC, mAD). The amount of IL-6 transported by pEVs, either on their surface or as cargo, was not different between the three groups (mean of 1.48 pg/mL, Figure 5h). In the presence of pEVs CTL, the level of IL-6 released by HMC3 cells after 24 h was similar to the PBS condition (180.34 and 145.99 pg/mL, respectively, Figure 5i) and consistent with previous observations (Dello Russo et al., 2018). Interestingly, in the presence of pEVs HeC, the release of IL-6 after 24 h of treatment (3 388.43 pg/mL) is higher than with LPS (648.5 pg/mL) or with 1  $\mu$ M of human  $\alpha A\beta_{1-42}$  (913.12 pg/mL). The effect of pEVs mAD on IL-6 was even greater (4 370.63 pg/mL). Given that bEnd.3 cells are murine endothelial cells, the quantification of IL-6 using a human-specific ELISA enabled us to detect only the cytokines released by human HMC3 cells plated in our in vitro BBB model. To eliminate the bias of IL-6 coming from pEVs, levels of IL-6 released by HMC3 cells in the presence of bEnd.3 murine cells on the Transwell device were normalized according to the amount transported by pEVs mAD. This confirmed that in the presence of the BBB model, IL-6 released by microglial cells was detectable on the abluminal side and to a lower extent on the luminal side (Figure 5j). These results suggest that the cytokine translocated the endothelial cells and circulated in the luminal chamber. Overall, HMC3 microglial cells produced and released high levels of pro-inflammatory cytokine IL-6 in response to the pEVs extracted from mAD patients.

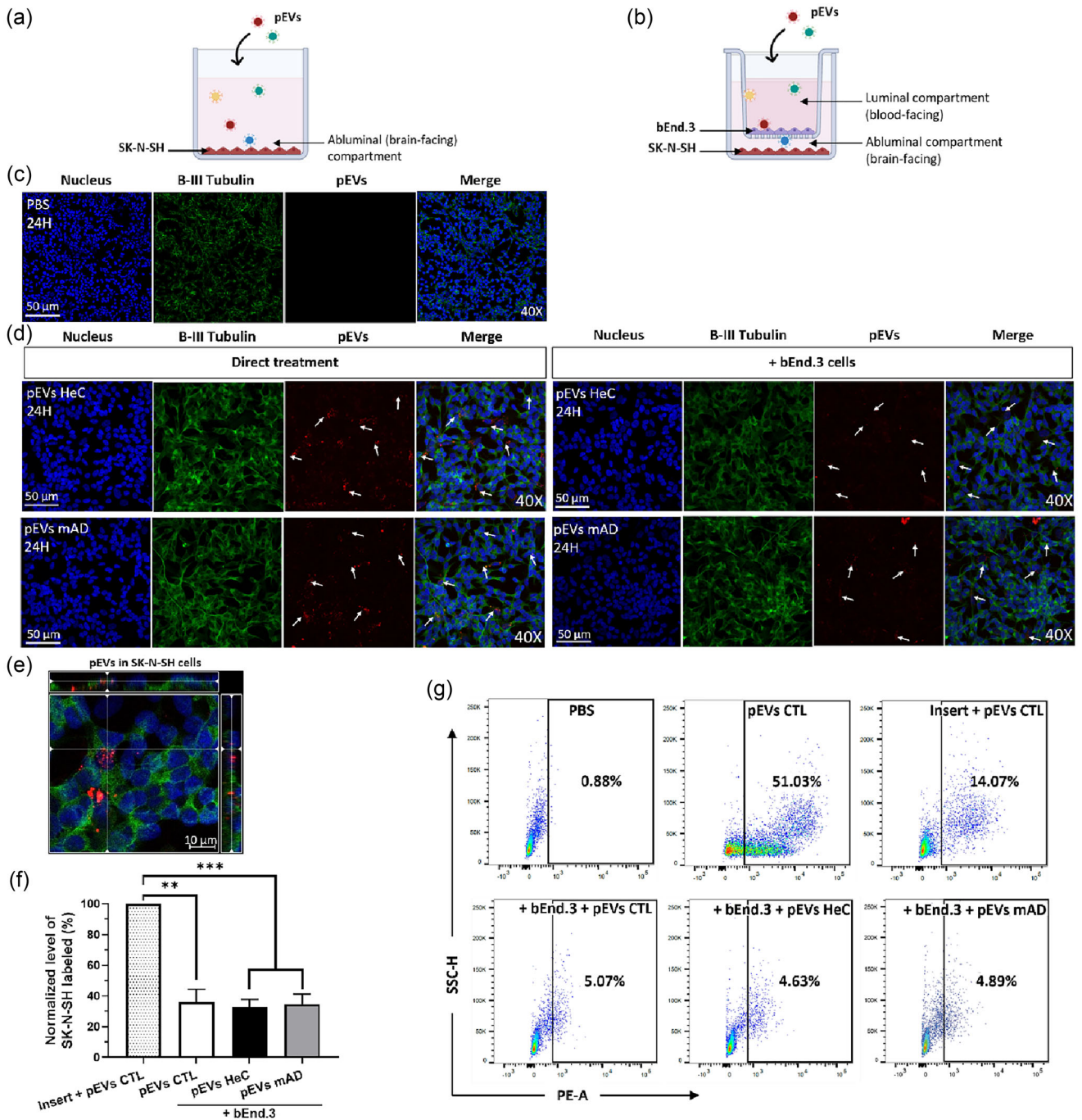


**FIGURE 3** Internalization of pEVs by SK-N-SH neuronal cells after their passage through bEnd.3 endothelial cells in vitro. (a) SK-N-SH cells were cultured at the bottom without or (b) with bEnd.3 cells seeded on a Transwell for 10 days, then  $1 \times 10^{10}$  pEVs/mL were added at the luminal side for 24 h. (c) Incubation with PBS for 24 h without PKH-pEVs. (d) Confocal imaging of PKH-pEVs (in red, indicated by arrows) internalized by SK-N-SH cells (nucleus in blue,  $\beta$ -III Tubulin in green) following a direct treatment or in the presence of bEnd.3 cells in the Transwell device. (e) Internalization of PKH-pEVs (in red, indicated by arrows) by SK-N-SH cells (40 $\times$ ). (f)–(g) Percentage of SK-N-SH cells internalizing PKH-pEVs quantified by flow cytometry and compared by ordinary one-way ANOVA, Tukey's multiple comparisons test. Prior statistical analysis, the normality of each data set was evaluated. Data are expressed in mean  $\pm$  SEM with \* $p \leq 0.5$ ; \*\* $p \leq 0.05$ ; \*\*\* $p \leq 0.005$ ; \*\*\*\* $p \leq 0.0005$  with  $n \geq 6$  per group. pEVs, peripheral EVs.

### 7.3 | Biodistribution of pEVs in zebrafish larvae and diffusion in the brain

The in vivo ability of pEVs to translocate across the blood vessel endothelium to the brain was evaluated in zebrafish larvae as in our previous studies (Oliveira Silva et al., 2024; Rabanel et al., 2021). To explore the interaction of pEVs with vascular endothelial cells in vivo, we used the *Tg(flk1:EGFP)* zebrafish model. To confirm the functionality and integrity of the BBB at 2 and 3 dpf,

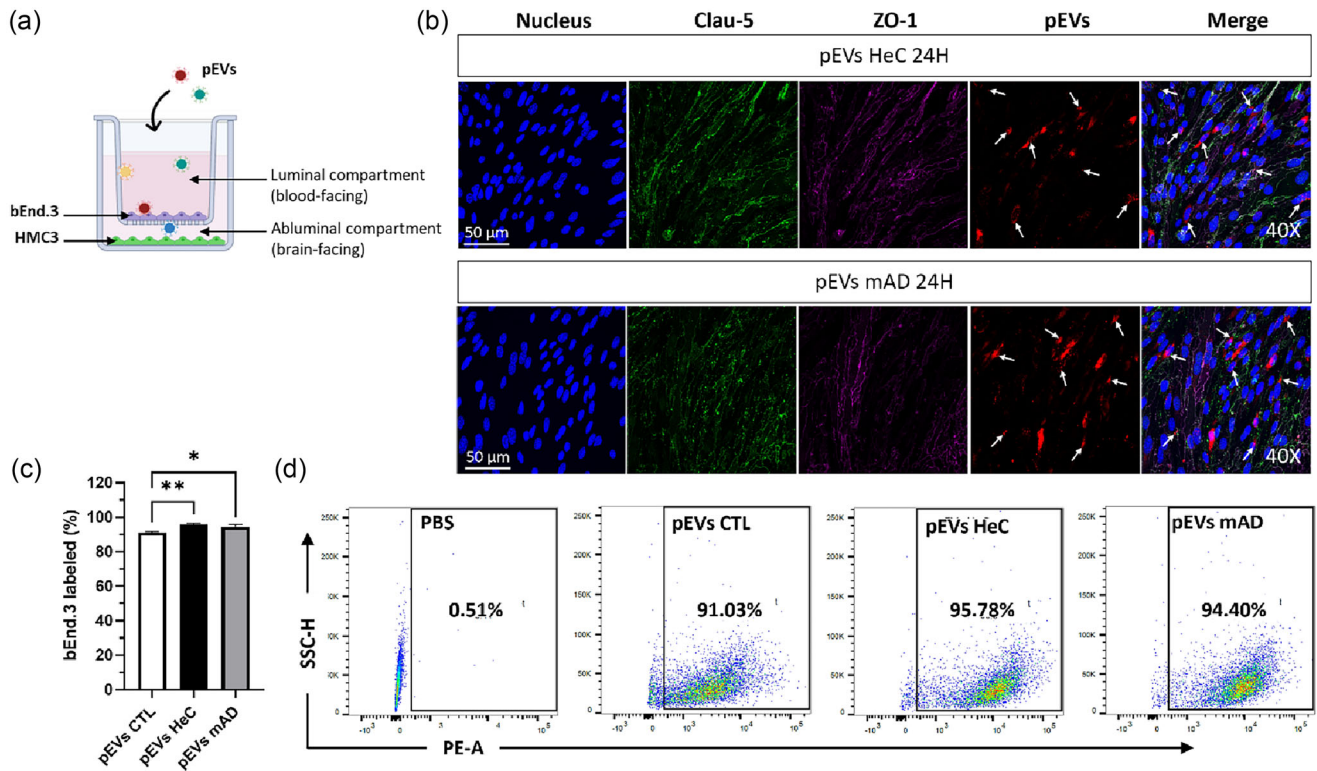


**FIGURE 4** Passage of pEVs through bEnd.3 endothelial cells in the presence of HMC3 microglial cells. (a) bEnd.3 cells were cultured on a Transwell for 10 days with HMC3 cells seeded at the bottom, and  $1 \times 10^{10}$  pEVs/mL were added for 24 h. (b) Uptake of PKH-pEVs (in red, indicated by arrows) by bEnd.3 cells (nuclei in blue, Clau-5 in green, ZO-1 in purple). (c)–(d) Percentage of bEnd.3 cells internalizing PKH-pEVs were quantified by flow cytometry and compared by ordinary one-way ANOVA. Prior statistical analysis, the normality of each data set was evaluated. Data are expressed in mean  $\pm$  SEM with  $^*p \leq 0.5$ ;  $^{**}p \leq 0.05$ ;  $^{***}p \leq 0.0005$  with  $n \geq 6$  per group. pEVs, peripheral EVs.

we conducted a series of preliminary experiments. The permeability of the small particles (10 kDa Dextran) through the blood vessels was validated, while larger particles (1 MDa Dextran) were excluded from the brain (Figures S5a,b). We further ascertained that the fluorescence detected in the brain when the peripheral injection of PKH-pEVs corresponds to pEVs (Figure S5b).

The biodistribution of human pEVs in zebrafish larvae was then assessed, focusing more specifically on pEVs from HeC and mAD subjects (Figure 6a). At 1-h post-injection (hpi), PKH-pEVs remained largely in the blood circulation (Figure 6b) with fluorescence being rapidly detected in the trunk blood vessels and the caudal venous plexus (CVP, Figures 6c,d). Interestingly, at 1 hpi, the brain distribution of pEVs was already visible and seemed to display a sub-cranial diffuse signal, likely around the developing choroid plexus (CP) (Figures 6c,e). Bright fluorescent spots corresponding to adherent and internalized pEVs in vascular endothelial cells were detected in the head (Figure S6a) and especially in the CVP (Figure S6b). However, we cannot exclude that the brighter red spots could also be attributed to CVP resident macrophages, which are known to engulf rapidly a large amount of particles such as pEVs (Hayashi et al., 2020). At 24 hpi, there was a marked increase of the fluorescence in the brain of *Tg(flk1:EGFP)* zebrafish compared to the signal recorded at 1 hpi, as confirmed by the analysis of the head-to-body fluorescence intensity ratio (Figure 6f). In vivo recording of the head at 20X revealed that even at 24 hpi, pEVs were still diffusing in the blood vessels, as confirmed by the fluorescent filaments observed in the circulation (Figure S6c).

At 1 hpi, imaging the head at 20X magnification further confirmed that pEVs were interacting with the endothelial cells and diffused outside the vessels into the brain (Figure 7a). Using the Imaris software, at 1 hpi we found that 23.32% of pEVs isolated from HeC and 13.70% of pEVs from mAD were interacting with endothelial cells in the recorded forebrain-midbrain area (Figures 7b,c,d). At 24 hpi, these interactions were evaluated to 28.15% for pEVs extracted from HeC and 19.53% for pEVs from mAD. The level of interaction between PKH-pEVs and endothelial cells remained consistent from 1 to 24 hpi (mean of 21.28%), suggesting a constant and progressive diffusion of pEVs through the endothelial cells over time. At 24 hpi, fluorescence leakage was still observed in trunk vessels, thereby confirming that pEVs were able to cross the BBB and reach the brainstem. The leakage of the fluorescence was apparent for both the vicinity of the major brain vessels and the microvessels.

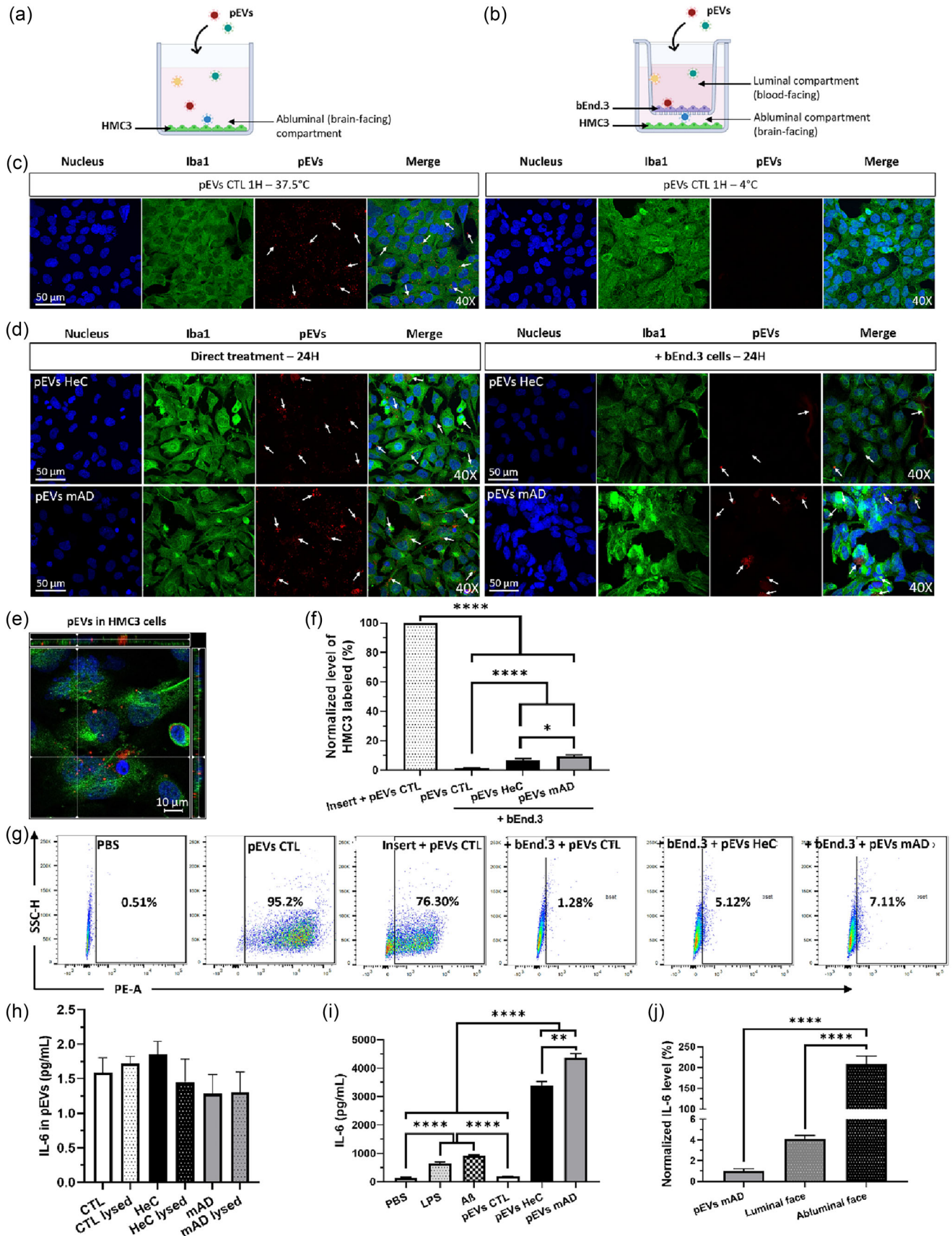


**FIGURE 5** Internalization of pEVs by HMC3 microglial cells after their passage through bEnd.3 endothelial cells. (a) HMC3 cells were cultured at the bottom without or (b) with bEnd.3 cells seeded on a Transwell for 10 days, then  $1 \times 10^{10}$  pEVs/mL were added at the luminal side for 24 h. (c) Internalization of

(Continues)

**FIGURE 5** (Continued)

PKH-pEVs (in red, indicated by arrows) by HMC3 cells (nuclei in blue, Iba1 in green) at 4°C and 37.5°C after 1-h and (d) 24 h incubation with or without bEnd.3 cells on the Transwell device. (e) Internalization of PKH-pEVs (in red) by microglial cells (nucleus in blue, Iba1 in green) confirmed by a z-axis plan (40×). (f) Percentages of HMC3 cells internalizing PKH-pEVs were quantified by flow cytometry and normalized according to the incubation of microglial cells with an insert and pEVs CTL in the luminal compartment. Results were compared by ordinary one-way ANOVA and Tukey's multiple comparisons test. (g) Percentages of HMC3 cells internalizing PKH-pEVs were quantified by flow cytometry. (h) Levels of IL-6 on pEV samples by ELISA and comparison by ordinary one-way ANOVA, Tukey's multiple comparisons test. (i) Quantification of IL-6 released by HMC3 cells in the media following 24 h of treatment with either PBS, LPS, A $\beta$  or pEVs. Comparison by ordinary one-way ANOVA, Tukey's multiple comparisons test. (j) Levels of IL-6 released by HMC3 cells in the presence of bEnd.3 cells and were normalized according to the amount transported by pEVs mAD. IL-6 levels were quantified into both compartments of the Transwell device and compared by ordinary one-way ANOVA, Tukey's multiple comparisons test. Prior statistical analysis, the normality of each data set was evaluated. Data are expressed in mean  $\pm$  SEM with \* $p \leq 0.05$ ; \*\* $p \leq 0.005$ ; \*\*\*\* $p \leq 0.0005$  with  $n \geq 6$  per group.

## 7.4 | Brain homing of pEVs in vivo conditions

To confirm that pEVs are taken up by cells rather than filling the extracellular space after crossing the BBB, analogous injections were performed in two transgenic lines Tg(*huc:eGFP*) and Tg(*gfap:eGFP*) displaying fluorescently labelled neuronal and glial-like cells at 2 dpf (Figures 8,9). The fluorescence was similar with or without both inhibitors of the endogenous release of EVs, Manumycin A and GW4869, indicating that the fluorescence corresponds to the PKH-pEVs injected in the zebrafish (Figure S7). The signal related to PKH-pEVs was similar with or without both inhibitors. PKH-pEVs were able to cross the BBB and be internalized by neuronal (Figure S7a) and glial-like cells (Figure S7b). At 1 hpi, neuronal and glial-like cells were filled with PKH-pEVs and were found confined within cell membranes, outside the vasculature (Figures 8a,d). As expected, most of the interactions of PKH-pEVs with neuronal and glial-like cells were close to the blood vasculature and the CP, which was confirmed by in vivo live imaging in the Tg(*huc:eGFP*) (Figures S8a, b, c, d, e) and the Tg(*gfap:eGFP*) models (Figures S9a, b, c), respectively. The internalization of pEVs from CTL (data not shown), HeC or mAD patients by these cells was continuous over time as they crossed the BBB (Figures 8b,e).

Interestingly, the amount of internalization of pEVs by glial-like cells was higher than that by neuronal cells. At 1 hpi, 3.47% to 4.44% of glial-like cells had internalized pEVs from HeC and mAD, respectively, which increased significantly to 19.37% for pEVs HeC at 24 hpi (Figures 8c,f). The level of internalization of pEVs mAD by glial-like cells was not different over time (Figure 8f). Adding up the percentages of internalization of pEVs with endothelial, neuronal and radial glial cells shows that at 1 hpi 28.04% of pEVs from HeC and 19.15% of pEVs from mAD were detectable in the head and interacting with at least three different cell types. At 24 hpi, these interactions increased up to 49.86% of pEVs from HeC and 31.77% of pEVs from mAD (Figure 9).

Finally, to study the distribution of pEVs once in the brain in a more complex animal model, pEVs were injected into the hippocampus of the mouse brain. A bi-lateral injection in the CA1 of  $2 \times 10^9$  PKH-pEVs derived from CTL patients was performed (Figure S10). At 30 min and 1 hpi, PKH-pEVs accumulated around the site of injection, in the circumventricular zones, the cortex, the hippocampus and in more distant cerebral areas, probably due to the irrigation by cerebral ventricles (Figure S10). With confocal imaging, we confirmed that several pEVs from CTL were captured by neurons and astrocytes, specifically in the hippocampus but also in some distant parts of the cortex (Figure S10b). These results indicate that once in the brain, pEVs diffused in different cerebral areas, notably via the ventricles and the CSF flow, and were internalized by mouse cerebral cells despite their human origin. These results also demonstrate that brain homing is species-independent.

## 8 | DISCUSSION

EVs have garnered significant interest in the past few years as they are transforming the conventional understanding of intercellular communication. Their capacity to transfer their molecular cargo to both neighbouring and distant recipient cells has been well documented, and pEVs are increasingly recognized as mediators of blood-brain bidirectional communication (Morad et al., 2019; van Niel et al., 2018). Recent studies suggest that the peripheral injection of EVs may selectively target and accumulate in pathologically relevant brain regions (Kur et al., 2020; Perets et al., 2019). It has been proposed that their homing mechanism could be inflammatory-driven (Perets et al., 2019) and triggered by neuronal activation (Kur et al., 2020). Previously, our research, along with that of others, has demonstrated that pEVs cargo differs between HeC and mAD (Haddad, Perrotte, Ben Khedher, et al., 2019; Haddad, Perrotte, Landri, et al., 2019; Haddad et al., 2021). However, the question of whether there is a difference in the permeability of pEVs through the BBB as well as their uptake by neuronal and microglial cells has not been yet investigated regarding AD pathogenesis. Furthermore, considering that pEVs have the potential to carry pathogenic, inflammatory, and oxidative markers (Ben Khedher et al., 2023; Haddad et al., 2021; Perrotte et al., 2020), it is imperative to ascertain whether pEVs from AD patients cross differently the BBB and propagate within the brain. This knowledge is crucial for apprehending the influence of peripheral disorders on the pathophysiology of AD. In this study, for the first time, it was demonstrated in in vitro and in vivo models that pEVs isolated from CTL, HeC and mAD patients cross the BBB, disseminate in the brain, and are



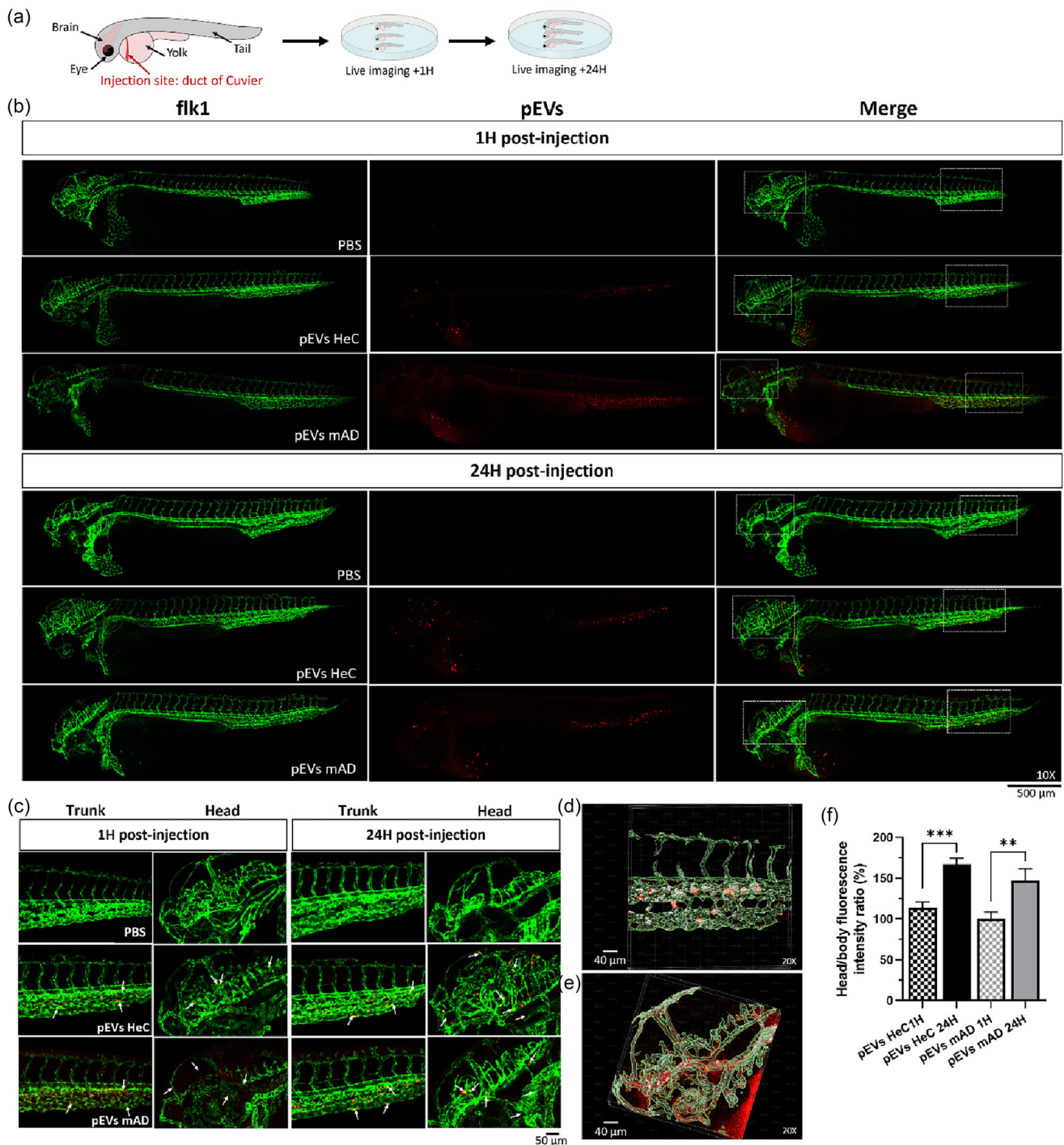


**FIGURE 6** In vivo biodistribution of pEVs in *Tg(flkl:EGFP)* zebrafish larvae at 2 dpf and 3 dpf. (a) 4.5 nL of PBS or pEVs from either HeC or mAD patients ( $1 \times 10^{10}$  pEVs/mL) were microinjected into the blood circulation of 2 days post-fertilization larvae, and the biodistribution was followed 1 and 24 hpi by in vivo confocal microscopy. (b) Live confocal images (maximum projection) at 1 and 24 hpi of zebrafish larva bodies (10 $\times$ ), with pEVs in red and blood vessels in green and (c) magnification of the head and the trunk, with red pEVs are indicated by arrows. (d) Three-dimensional reconstruction on Imaris software of the trunk and (e) the head of a zebrafish larvae 1 hpi of PKH-pEVs. Endothelial cells are in green, PKH-pEVs from HeC patients are in red, and colocalization areas are in white. (f) Quantification of the head-to-total body fluorescence intensity ratio was performed using Zen 2.6 software, and comparisons were made using ordinary one-way ANOVA followed by Tukey's multiple comparisons test. Prior statistical analysis, the normality of each data set was evaluated. Data are expressed in mean  $\pm$  SEM  $^{**}p \leq 0.05$ ;  $^{***}p \leq 0.005$  with  $n = 7$  per group.

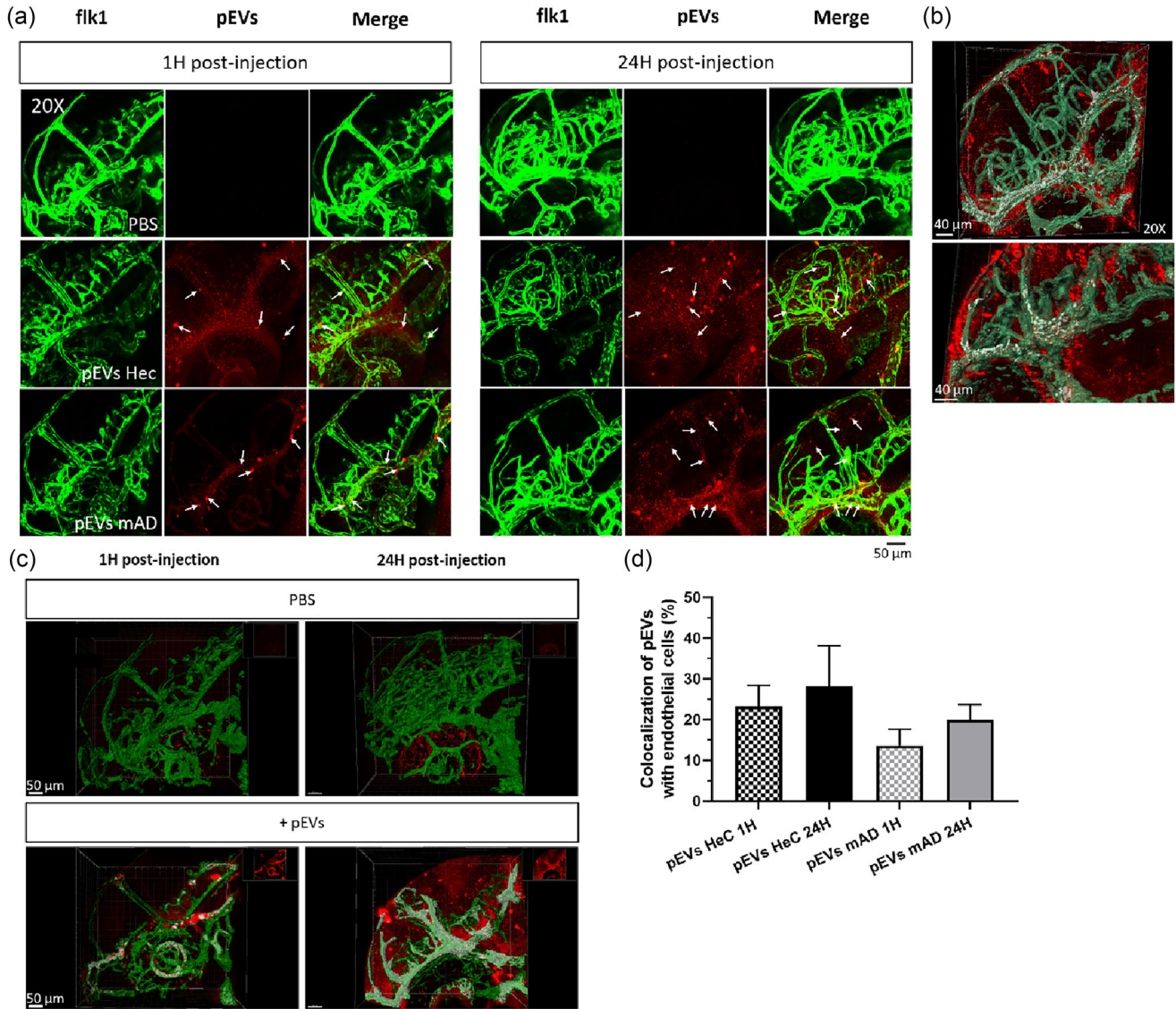


**FIGURE 7** Internalization of pEVs by endothelial cells in *Tg(flk1:EGFP)* zebrafish larvae at 2 and 3 dpf and brain homing. 4.5 nL of PBS or pEVs from either HeC or mAD patients ( $1 \times 10^{10}$  pEVs/mL) were microinjected into the blood circulation of 2 days post-fertilization larvae, and the biodistribution was followed 1 and 24 hpi by in vivo confocal microscopy. (a) Live confocal images (maximum projection) at 1 and 24 hpi of the head of zebrafish larvae (20X) after injection of either PBS or pEVs (in red, indicated by arrows). Endothelial cells are in green. (b)–(c) Three-dimensional reconstruction on Imaris software of the head of the zebrafish in control (CTL) condition or 1 and 24 hpi of PKH-pEVs. Endothelial cells are in green, PKH-pEVs from mAD patients are in red, and colocalization areas are in white. (d) The percentage of internalization of PKH-pEVs by endothelial cells was quantified by using Imaris software and analysed by ordinary one-way ANOVA followed by Tukey's multiple comparisons test. Prior statistical analysis, the normality of each data set was evaluated with  $n = 7$  per group.

internalized by neuronal and microglial cells. Interestingly, pEVs can induce the release of the pro-inflammatory cytokine IL-6 by microglial cells, with higher release being observed in the presence of pEVs from mAD. We also demonstrated in a mouse model that once pEVs reach the CA1 area of the hippocampus, they spread to the cortex, which is consistent with the hypothesis that EVs can disseminate Tau (Ruan et al., 2021) and  $A\beta$  in these cerebral areas (Beretta et al., 2020).

Our data showed a decline in pEVs levels in the serum with age, whereas AD patients showed a notable increase in pEVs levels. All samples were treated in an identical manner throughout the collection and storage process. Consequently, the observed variation in size and concentration can be solely attributed to biological effects. The levels of pEVs in the bloodstream are determined by a dynamic balance between their secretion by different cells in the bloodstream and from different organs, and their clearance rates. They are likely cleared by B cells, monocytes (Eitan et al., 2017) and macrophages (Matsumoto et al., 2020). Given that phagocytosis by macrophages (Moss et al., 2023) and monocytes are known to be reduced with age (Solana et al., 2012), the decrease of pEVs levels observed in this study in older individuals could be due to their increased internalization by B-cells (Eitan et al., 2017). However, we cannot exclude a decrease in their biogenesis and secretion in cognitively healthy elderly

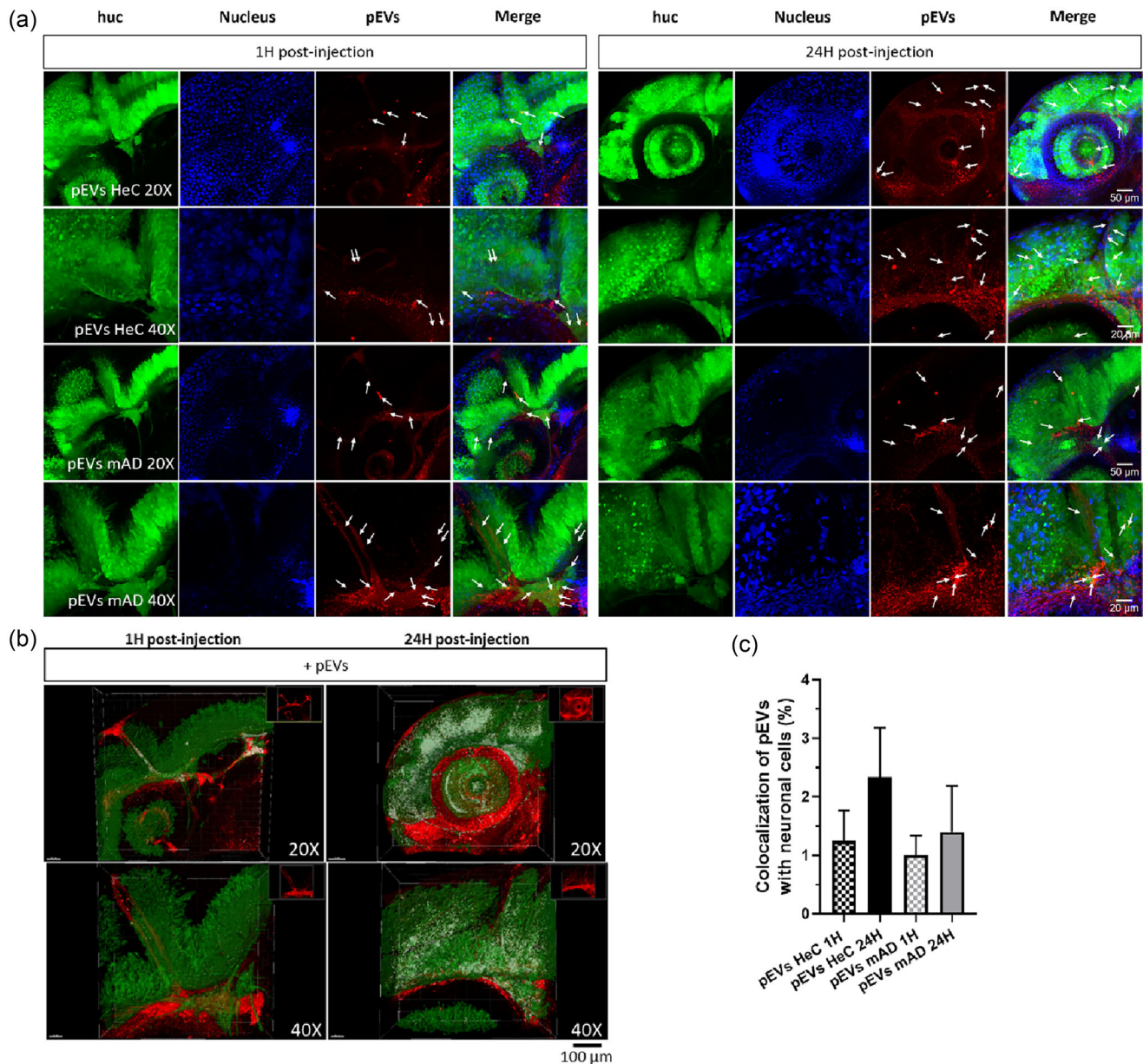


**FIGURE 8** Brain homing of pEVs and their internalization by neuronal cells in the *Tg(huc:EGFP)* zebrafish. (a) Live confocal images (maximum projection) at 1 hpi and 24 hpi of the head of *Tg(huc:EGFP)* larvae (20× and 40×) after injection of 4.5 nL of PBS or pEVs ( $1 \times 10^{10}$  pEVs/mL) from either HeC or mAD patients (red, indicated by arrows). Neurons are in green and the nucleus in blue. (b) Three-dimensional reconstruction on Imaris software of the head of the zebrafish 1 and 24 hpi of PKH-pEVs from HeC (20×) and mAD (40×) patients. Neuronal cells are in green, PKH-pEVs are in red, and colocalization areas are in white. (c) The percentage of neurons engulging PKH-pEVs was quantified by Zen 2.6 software and compared by ordinary one-way ANOVA followed by Tukey's multiple comparisons test.

subjects. Conversely, it could be observed that pEVs levels are increased in mAD as it has been described in other diseases with systemic inflammation (Ben Khedher et al., 2021; Zhou et al., 2014). This suggests that the EVs biogenesis is enhanced, either to expel toxic compounds from the cells, or to increase the signalling communications between cells, which may contribute to the disease progression (Zhou et al., 2014). For instance, it is established that in response to an infection, platelets release a greater number of EVs in the bloodstream (Kerris et al., 2020). Similarly, in metabolic disorders, the liver, pancreas, platelets, endothelial cells, erythrocytes and lymphocytes released more EVs into the bloodstream than in healthy subjects (Crewe, 2023; Htike et al., 2019). Further investigation of the biogenesis of EVs from peripheral organs may offer deeper insight into the aetiology of AD.

Interestingly, pEVs from CTL, HeC and mAD patients exhibit different zeta potential data, displaying a diminished negative charge with age (−11.95 and −15.03 mV). pEVs from young CTL donors without metabolic disorders have a zeta potential of −19.15 mV, which is considered as anionic and within the optimal range for biological membranes. This observation suggests that their enrichment did not alter their property and is not toxic. Since most cellular membranes are negatively charged, anionic

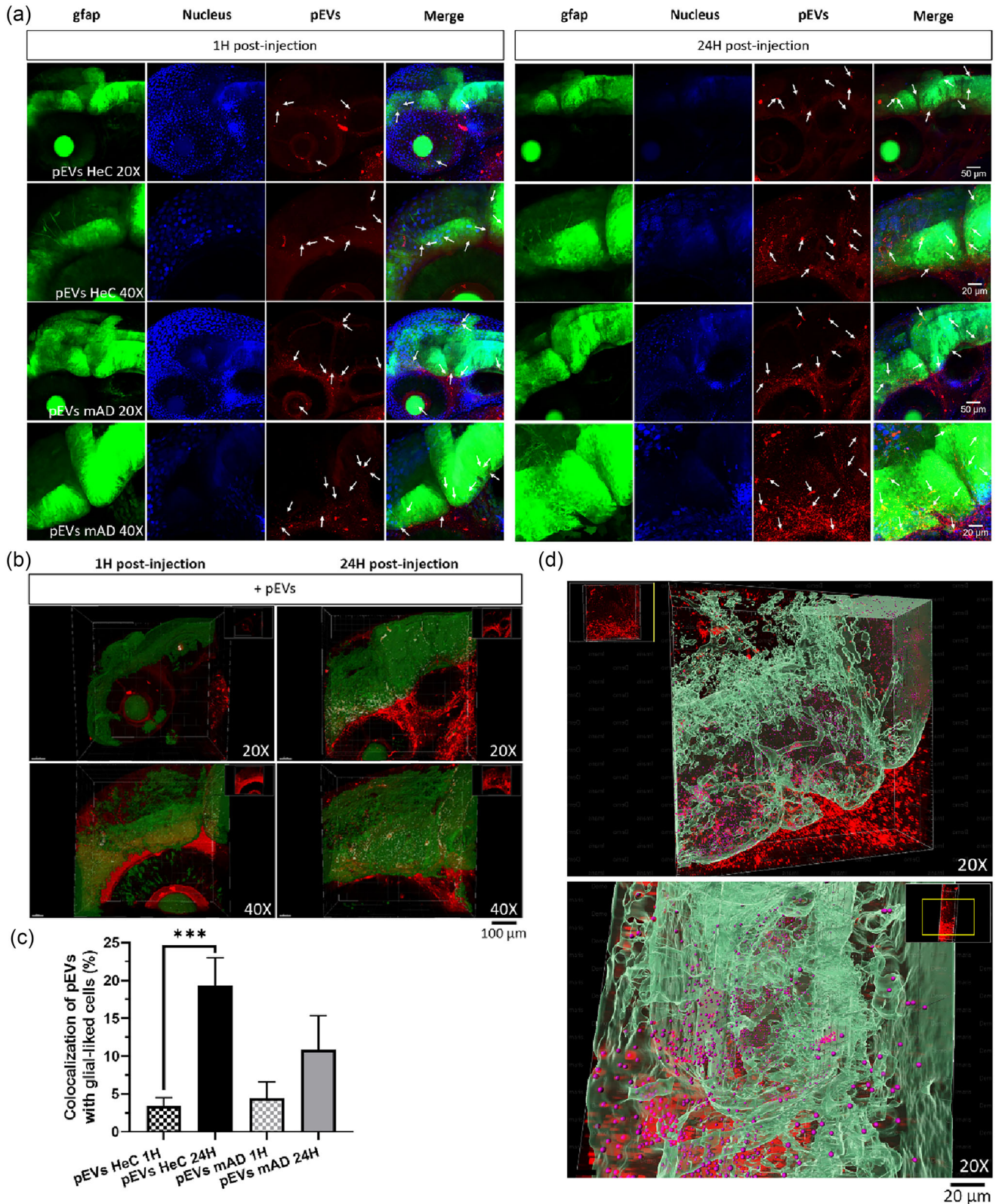


**FIGURE 9** Brain homing of pEVs and their internalization by glial-like cells in the *Tg(gfap:EGFP)* zebrafish. (a) Live confocal images (maximum projection) at 1 and 24 hpi of the head of *Tg(gfap1:EGFP)* larvae (20 $\times$  and 40 $\times$ ), with pEVs in red (indicated by arrows) and glial-like cells in green. (b) Three-dimensional reconstruction on Imaris software of the head of the zebrafish 1 and 24 hpi of PKH-pEVs from HeC (20 $\times$ ) and mAD (40 $\times$ ) patients. Glial-like cells are in green, PKH-pEVs are in red, and colocalization areas are in white. (c) The percentage of glial-like cells capturing PKH-pEVs was quantified by Zen 2.6 software and compared by ordinary one-way ANOVA followed by Tukey's multiple comparisons test. (d) Three-dimensional reconstruction on Imaris software of PKH-pEVs diffusion into the brain and their internalization by glial-like cells 24 hpi. Prior statistical analysis, the normality of each data set was evaluated. Data are expressed in mean  $\pm$  SEM \*\*\* $p \leq 0.05$ ; \*\*\*\* $p \leq 0.005$  with  $n = 7$  per group.

particles are generally less toxic to the cell wall (Clogston & Patri, 2011). As the surface interactions of EVs may regulate their organ and cellular tropism, immune recognition, and cellular uptake (Buzás et al., 2018), a lower zeta potential could reflect: (1) a lower dispersion stability of the pEVs and (2) a change in the protein corona. *In fine*, it may compromise their biological function (Bhattacharjee, 2016). In numerous reports, the protein corona formed on human pEVs are typically composed of complement proteins and apolipoproteins such as ApoA1, ApoB, ApoC3, ApoE, complement factors 3 and 4B, fibrinogen  $\alpha$ -chain, immunoglobulin heavy constant  $\gamma$ 2 and  $\gamma$ 4 chains (Tóth et al., 2021). In addition to the aforementioned proteins, our recent findings have demonstrated that  $\alpha$ A $\beta$ <sub>1-42</sub>, ApoJ and RAGE were also bound to the external layer of pEVs originating from AD patients (Ben Khedher et al., 2023). It can be inferred that the biodistribution and internalization of pEVs may be attributed to proteins and glycoproteins present on the surface of both the vesicle and the target cell (Mulcahy et al., 2014), whereas the transcytosis of pEVs may depend on their size and density (Morad et al., 2019). Consequently, this could impact their interaction with endothelial cells and their passage to the brain. Our results showed that pEVs derived from mAD patients seem to compromise the integrity of the bEnd.3 cells cultured in a Transwell device as evidence by a reduction of the TEER which is comparable to observations in some pathological conditions (Nair et al., 2023; Park et al., 2023). A similar reduction in the TEER was previously observed in the presence of inflammatory stimuli, such as LPS or TNF- $\alpha$  (Matsumoto et al., 2017; Sun et al., 2022). As pEVs derived from mAD patients did not alter the expression of tight-junction proteins ZO-1 and Clau-5, the reduction in the TEER could be due to an alteration of the ionic conductance of the paracellular pathway (Liu et al., 2024).

Our results showed that a mere one-third of pEVs are released by bEnd.3 cells. Subsequently, the uptake of pEVs by microglia cells increased with age and was higher for pEVs deriving from mAD compared to those from CTL and HeC patients, whereas neuronal cells showed similar levels of uptake across all pEVs sources, regardless of their origins. This suggests a beneficial role of microglia-mediated clearance of pEVs containing higher levels of pathological cargo such as pTau and A $\beta$  (Perrotte et al., 2020). It is noteworthy that after 24 h of incubation, the percentage of pEVs-PKH26 was found to be lower in HMC3 cells than in SK-N-SH cells, suggesting that microglia may clear pEVs at a higher rate than neuronal cells. Our results are in accordance with findings by Xia et al., who showed a higher uptake of pEVs from Parkinson's disease by microglial cells in mice, which were completely cleared possibly through autophagy after 24 h (Xia et al., 2019). Interestingly, in the presence of the bEnd.3 cells and following a 24-h treatment with pEVs derived from mAD patients, HMC3 cells underwent morphological transition from a resting ramified shape to an activated amoeboid phenotype. This amoeboid phenotype has been previously described in response to A $\beta$  in this cell line (Akhter et al., 2021), reflecting a change in microglial cell activity due to an inflammatory-like trigger. In our study, this morphological change may be attributed to a dual effect: (1) the cargo of the pEVs derived from mAD patients and (2) the compromised bEnd.3 endothelial cells, which may release pathogenic mediators such as EVs. Conversely, microglial cells may release other pathogenic mediators which could compromise the bEnd.3 integrity and participate to the TEER reduction. In this regard, our results show that pEVs from mAD patients induce a huge release of IL-6, higher than LPS or  $\alpha$ A $\beta$ <sub>1-42</sub>.

Secreted IL-6 can, in turn, activate microglia (Lin et al., 2022), increase APP expression (Akiyama et al., 2000), deregulate the cdk5/p35 pathway resulting in abnormal hyperphosphorylation of Tau protein (West et al., 2022), being deleterious for neurons (Rothaug et al., 2016). It has been demonstrated that in addition to exerting pleiotropic effects on inflammation, immune response, and haematopoiesis, the increase in the expression and secretion of IL-6 can be associated with various neurological disorders, including AD (Akhter et al., 2021). In AD patients, elevated levels of IL-6 have been reported in the plasma, cerebrospinal fluid, and brain parenchyma (Galimberti et al., 2008; Licastro et al., 2000; Swardfager et al., 2010). Our results suggest that microglia activation may contribute to the elevated level of IL-6 observed in the blood circulation. In addition, high levels of IL-6 participate in the disruption of BBB integrity (Blecharz-Lang et al., 2018), which could be in part responsible for the TEER reduction observed with pEVs from mAD patients. Therefore, our results suggest that pEVs from elderly subjects and, more notably, from mAD patients which display a distinctive signature (Ben Khedher et al., 2023; Haddad, Perrotte, Landri, et al., 2019; Perrotte et al., 2020), have the capacity to activate microglia, contribute to the induction of inflammation and promote AD pathogenesis. This is of particular interest because brain-derived EVs have been demonstrated to play a dual role through their involvement in neuroprotective and neurodegenerative pathways (Clayton et al., 2021; Fröhlich et al., 2014). On one hand, they can mitigate disease mechanisms, notably by transferring neuroprotective substances between cells (Long et al., 2020). On the other hand, they have been demonstrated to accelerate disease progression by facilitating the transfer of toxic proteins, promoting neuronal loss, and contributing to neuroinflammation (Gabielli et al., 2022). The findings of this study indicate that pEVs could contribute to early brain changes associated with AD, particularly in patients experiencing chronic peripheral inflammation (Ng et al., 2016).

To further assess the *in vivo* transport across the BBB and brain homing of pEVs, intravascular injections of pEVs were performed on the zebrafish, an excellent model to monitor the systemic circulation of particles, as well as interactions of particles with blood vessels (Rabanel et al., 2020). Using the Tg(*flkl:EGFP*) model, we demonstrated that injected pEVs distributed in a few seconds in the body and remained detectable for at least 24 h. The half-life of EVs in the bloodstream remains a topic of debate, with estimates ranging from a few minutes to hours due to their clearance by phagocytic cells, including macrophages and neutrophils (Imai et al., 2015). Given that our pEVs were isolated from the blood, they may present specific decorations that could increase their half-life, notably by acting as a 'don't eat me' signal or by targeting other cell types (Kamerkar et al., 2017). It has been well documented that the major tissue distribution of systemically administered EVs includes the liver, spleen, kidney,

lung, and gastrointestinal tract (Varga et al., 2016). This distribution is dependent on numerous factors such as the cellular origin of EVs, the composition of their vesicular membrane and the pathological condition of the host. It is worth noting that previous studies, including ours, have consistently detected the detected only small amounts of CNS-derived EV within the blood circulation (Goetzl et al., 2016; Perrotte et al., 2020; Visconte et al., 2023). Our findings revealed that pEVs were mostly found in specific areas, particularly the trunk blood vessels, the CVP, and the brain. The tropism of EVs in the CVP region is likely due to the patrolling of macrophages in this tortuous area (Hyenne et al., 2019). The CVP region is also considered functionally equivalent to a foetal liver, with vascular endothelial cells expressing scavenger receptors on their surface (Hayashi et al., 2020) that are responsible for the capture of particles (Campbell et al., 2018). The accumulation of fluorescent pEVs into the cardinal vein was observed at both 1 and 24 hpi, suggesting that some pEVs are engulfed by the scavenging endothelium receptors. Interestingly, we observed that levels of exogenous pEVs increase with time in the head, with no discernible difference between pEVs derived from HeC and mAD patients. This accumulation of exogenous pEVs over time was not observed in the periphery.

In vivo, evidence demonstrated that pEVs were able to translocate across the blood vessel endothelium and accumulate progressively over time in the brain. At 24 hpi, trunk vessels still demonstrated fluorescence leakage confirming that pEVs can pass through the blood vessels to the brain region. Leakage was apparent around the major brain vessels and even the microvessels, which are known to display tight-junction complexes (Jeong et al., 2008). This indicates that the blood-brain passage is an active transcellular transport rather than a passive paracellular diffusion. The Tg(*flk1:EGFP*) model revealed that pEVs reach the brain *via* the endothelial cells. However, alternative pathways such as through the developing CP (Henson et al., 2014) cannot be excluded in this process. In the zebrafish, the CP possesses size-selective barrier properties as well as transporter activity (Henson et al., 2014), and might be involved in EV brain delivery as in mammals (Pauwels et al., 2022).

With the two transgenic zebrafish models Tg(*huc:EGFP*) and Tg(*gfap:EGFP*), we showed that pEVs were rapidly internalized (in less than 1-h) by neuronal and glial-like cells, rather than remaining in the extracellular space following their translocation across the BBB. The Tg(*huc:EGFP*) line is a powerful genetic model that allows real-time visualization of the fate of pEVs by living neurons in vivo (Park et al., 2000). Similarly, Tg(*gfap:EGFP*) line is an interesting model as it exhibits labelled glial-like cells with complex branched morphology remarkably similar to those observed in mammals (Chen et al., 2020). These cells are in contact neurons, synapses and microvasculature, but they do not exhibit the classic stellar morphology of astrocytes and lack polarization of Aqp4 (Grupp et al., 2010; Jeong et al., 2008). Instead, they express GFAP-positive radial glial cells (Grupp et al., 2010). The majority of neuronal and glial-like cells associated with PKH-pEVs were located in close proximity to the blood vasculature and the CP. Analysis by the Imaris software revealed that the internalization of pEVs by glial-like cells was 10 times higher than by neurons, reaching a maximum after 1-h for pEVs from mAD patients probably due to a higher clearance. Interestingly, a great number of pEVs were found in low-density brain areas such as the pallium, which is a cerebral area similar to the hippocampus in mammals (Vaz et al., 2019).

Moreover, our confocal analysis indicated that labelled pEVs appeared to diffuse progressively into the skin of the zebrafish head. This diffusion was probably due to the presence of a lymphatic vessel network on the inner lining of the zebrafish skull (Castranova et al., 2021), which is similar to the meningeal lymphatic system found across mammals (van Lessen et al., 2017). While the mammalian glymphatic-paravascular clearance mechanism is a vascular entity involved in physiological and pathological conditions such as AD (Han et al., 2021), our results suggest that they are involved in pEVs clearance in the zebrafish model.

Finally, the dissemination of pEVs in the brain and their internalization by NeuN-positive neurons and GFAP-positive astrocytes were validated in the mouse brain. Once in the hippocampus, pEVs can spread in the different parts of its structure, as well as the cerebellum and the CP. Similarly, other studies reported the same tropism by injecting PKH-labelled sEVs in the lateral ventricles (Grapp et al., 2013) or in the tail vein of WT mice (Morales-Prieto et al., 2022). Furthermore, it has been demonstrated that pEVs isolated from the blood of aged mice can traverse the BBB and activate the glial cells of young mice (Morales-Prieto et al., 2022). Altogether, these results and ours reinforce the notion that pEVs can contribute to neuroinflammation. Thus, these results pave the way to novel mechanisms in AD pathogenesis and therapeutic targets by modulating peripheral inflammation.

## 9 | CONCLUSION

The current evidence suggests that AD is not a neuron-dominant disease. Instead, it appears that brain-dwelling non-neuronal cells and peripheral immune cells play a key role. Accordingly, a paradigmatic shift is needed to consider AD as a systemic disease. EVs have attracted considerable interest for their involvement in intercellular communication. However, previous studies have suggested that EVs transfer from the peripheral circulation to the CNS is uncommon under physiological conditions, with EVs accumulating in the liver, kidney, and spleen. The present study demonstrates that pEVs from adults, cognitively healthy elderly and AD patients can cross the BBB and reach the brain in vitro and in vivo. For the first time, we have highlighted the role of pEVs, particularly from AD patients, in microglial reactivity and its potential impact on AD through IL-6 secretion and BBB disruption. Our results put forward the hypothesis that systemic disorders, through pEVs, may trigger or accelerate the

progression of AD, which paved the way for novel therapeutic targets by modulating peripheral inflammation, pEVs biogenesis or translocation through the BBB.

## AUTHOR CONTRIBUTIONS

**Hermine Council:** Conceptualization (lead); data curation (lead); formal analysis (lead); investigation (lead); methodology (lead); project administration (supporting); resources (lead); software (lead); supervision (lead); validation (equal); visualization (lead); writing - original draft (lead); writing—review and editing (lead). **Rummenige Oliveira Silva:** Methodology (supporting); writing—review and editing (supporting). **Jean-Michel Rabanel:** Formal analysis (supporting); methodology (supporting); writing—review and editing (supporting). **Charlotte Zaouter:** Methodology (supporting); resources (supporting). **Mohamed Haddad:** Data curation (supporting); methodology (supporting); writing—review and editing (supporting). **Mohamed Raâfet Ben Khedher:** Resources (supporting). **Davide Brambilla:** Resources (supporting). **Tamas Fülöp:** Resources (supporting); writing—review and editing (supporting). **Shunmoogum A. Patten:** Conceptualization (supporting); resources (supporting); writing—review and editing (supporting). **Charles Ramassamy:** Conceptualization (supporting); funding acquisition (lead); project administration (lead); resources (supporting); supervision (lead); validation (equal); writing—review and editing (supporting).

## ACKNOWLEDGEMENTS

This study received support from the Research Chair Louise & André Charron on Alzheimer's disease, Canadian Institute of Health Research, NSERC/CRSNG, and Canada Foundation for Innovation. The authors express gratitude to Pr Davide Brambilla for the Cytoflex availability and to Pr Xavier Banquy for the access to the Institute for Research in Immunology and Cancer platform. We also thank Jessy Tremblay (INRS, Armand-Frappier Health Biotechnology Center) for assistance with experiments involving flow cytometry and confocal microscopy, and Arnaldo Nakamura (INRS, Armand-Frappier Health Biotechnology Center) for assistance with the transmission electron microscope. Cartoons in graphical abstract and figures 2A, 3A, 4A, S3A, S10A were created with BioRender.com.

## CONFLICT OF INTEREST STATEMENT

The authors have no relevant financial or non-financial interests to disclose and declare no competing interests.

## ORCID

Hermine Council  <https://orcid.org/0000-0003-2041-5134>

Charles Ramassamy  <https://orcid.org/0000-0002-3252-5878>

## REFERENCES

- Akhter, R., Shao, Y., Formica, S., Khrestian, M., & Bekris, L. M. (2021). TREM2 alters the phagocytic, apoptotic and inflammatory response to A $\beta$ (42) in HMC3 cells. *Molecular Immunology*, 131, 171–179. <https://doi.org/10.1016/j.molimm.2020.12.035>
- Akiyama, H., Barger, S., Barnum, S., Bradt, B., Bauer, J., Cole, G. M., Cooper, N. R., Eikelenboom, P., Emmerling, M., Fiebich, B. L., Finch, C. E., Frautschy, S., Griffin, W. S., Hampel, H., Hull, M., Landreth, G., Lue, L., Mrak, R., Mackenzie, I. R., ... Wyss-Coray, T. (2000). Inflammation and Alzheimer's disease. *Neurobiology of Aging*, 21(3), 383–421. [https://doi.org/10.1016/s0197-4580\(00\)00124-x](https://doi.org/10.1016/s0197-4580(00)00124-x)
- Banks, W. A., Sharma, P., Bullock, K. M., Hansen, K. M., Ludwig, N., & Whiteside, T. L. (2020). Transport of extracellular vesicles across the blood-brain barrier: Brain pharmacokinetics and effects of inflammation. *International Journal of Molecular Sciences*, 21(12), 4407. <https://doi.org/10.3390/ijms21124407>
- Ben Khedher, M. R., Haddad, M., Fulop, T., Laurin, D., & Ramassamy, C. (2023). Implication of circulating extracellular vesicles-bound amyloid- $\beta$ 42 oligomers in the progression of Alzheimer's disease. *Journal of Alzheimer's Disease*, 96(2), 813–825. <https://doi.org/10.3233/jad-230823>
- Ben Khedher, M. R., Haddad, M., Laurin, D., & Ramassamy, C. (2021). Apolipoprotein E4-driven effects on inflammatory and neurotrophic factors in peripheral extracellular vesicles from cognitively impaired, no dementia participants who converted to Alzheimer's disease. *Alzheimer's & Dementia: Translational Research & Clinical Interventions*, 7(1), e12124. <https://doi.org/10.1002/trc2.12124>
- Beretta, C., Nikitidou, E., Streubel-Gallasch, L., Ingelsson, M., Sehlin, D., & Erlandsson, A. (2020). Extracellular vesicles from amyloid- $\beta$  exposed cell cultures induce severe dysfunction in cortical neurons. *Scientific Reports*, 10(1), 19656. <https://doi.org/10.1038/s41598-020-72355-2>
- Bhattacharjee, S. (2016). DLS and zeta potential—What they are and what they are not? *Journal of Controlled Release*, 235, 337–351. <https://doi.org/10.1016/j.jconrel.2016.06.017>
- Blecharz-Lang, K. G., Wagner, J., Fries, A., Nieminen-Kelhä, M., Rösner, J., Schneider, U. C., & Vajkoczy, P. (2018). Interleukin 6-mediated endothelial barrier disturbances can be attenuated by blockade of the IL6 receptor expressed in brain microvascular endothelial cells. *Translational Stroke Research*, 9(6), 631–642. <https://doi.org/10.1007/s12975-018-0614-2>
- Butovsky, O., & Weiner, H. L. (2018). Microglial signatures and their role in health and disease. *Nature Reviews Neuroscience*, 19(10), 622–635. <https://doi.org/10.1038/s41583-018-0057-5>
- Buzás, E. I., Tóth, E. Á., Sódar, B. W., & Szabó-Taylor, K. É. (2018). Molecular interactions at the surface of extracellular vesicles. *Seminars in Immunopathology*, 40(5), 453–464. <https://doi.org/10.1007/s00281-018-0682-0>
- Campbell, F., Bos, F. L., Sieber, S., Arias-Alpizar, G., Koch, B. E., Huwyler, J., Kros, A., & Bussmann, J. (2018). Directing nanoparticle biodistribution through evasion and exploitation of Stab2-dependent nanoparticle uptake. *ACS Nano*, 12(3), 2138–2150. <https://doi.org/10.1021/acsnano.7b06995>
- Castranova, D., Samasa, B., Galanternik, M. V., Jung, H. M., Pham, V. N., & Weinstein, B. M. (2021). Live imaging of intracranial lymphatics in the zebrafish. *Circulation Research*, 128(1), 42–58. <https://doi.org/10.1161/CIRCRESAHA.120.317372>

- Chen, C. C., Liu, L., Ma, F., Wong, C. W., Guo, X. E., Chacko, J. V., Farhoodi, H. P., Zhang, S. X., Zimak, J., Ségaliny, A., Riazifar, M., Pham, V., Digman, M. A., Pone, E. J., & Zhao, W. (2016). Elucidation of exosome migration across the blood-brain barrier model in vitro. *Cellular and Molecular Bioengineering*, 9(4), 509–529. <https://doi.org/10.1007/s12195-016-0458-3>
- Chen, J., Poskanzer, K. E., Freeman, M. R., & Monk, K. R. (2020). Live-imaging of astrocyte morphogenesis and function in zebrafish neural circuits. *Nature Neuroscience*, 23(10), 1297–1306. <https://doi.org/10.1038/s41593-020-0703-x>
- Clayton, K., Delpech, J. C., Herron, S., Iwahara, N., Ericsson, M., Saito, T., Saido, T. C., Ikezu, S., & Ikezu, T. (2021). Plaque associated microglia hyper-secrete extracellular vesicles and accelerate tau propagation in a humanized APP mouse model. *Molecular Neurodegeneration*, 16(1), 18. <https://doi.org/10.1186/s13024-021-00440-9>
- Clogston, J. D., & Patri, A. K. (2011). Zeta potential measurement. *Methods in Molecular Biology*, 697, 63–70. [https://doi.org/10.1007/978-1-60327-198-1\\_6](https://doi.org/10.1007/978-1-60327-198-1_6)
- Counil, H., & Krantic, S. (2020). Synaptic activity and (neuro)inflammation in Alzheimer's disease: Could exosomes be an additional link? *Journal of Alzheimer's Disease*, 74(4), 1029–1043. <https://doi.org/10.3233/jad-191237>
- Craig, M. P., Gilday, S. D., Dabiri, D., & Hove, J. R. (2012). An optimized method for delivering flow tracer particles to intravital fluid environments in the developing zebrafish. *Zebrafish*, 9(3), 108–119. <https://doi.org/10.1089/zeb.2012.0740>
- Crewe, C. (2023). Energetic stress-induced metabolic regulation by extracellular vesicles. *Comprehensive Physiology*, 13(3), 5051–5068. <https://doi.org/10.1002/cphy.c230001>
- Dello Russo, C., Cappoli, N., Coletta, I., Mezzogori, D., Paciello, F., Pozzoli, G., Navarra, P., & Battaglia, A. (2018). The human microglial HMC3 cell line: Where do we stand? A systematic literature review. *Journal of Neuroinflammation*, 15(1), 259. <https://doi.org/10.1186/s12974-018-1288-0>
- Dinkins, M. B., Dasgupta, S., Wang, G., Zhu, G., & Bieberich, E. (2014). Exosome reduction in vivo is associated with lower amyloid plaque load in the 5XFAD mouse model of Alzheimer's disease. *Neurobiology of Aging*, 35(8), 1792–1800. <https://doi.org/10.1016/j.neurobiolaging.2014.02.012>
- Dinkins, M. B., Enasko, J., Hernandez, C., Wang, G., Kong, J., Helwa, I., Liu, Y., Terry, A. V., Jr., & Bieberich, E. (2016). Neutral sphingomyelinase-2 deficiency ameliorates Alzheimer's disease pathology and improves cognition in the 5XFAD mouse. *Journal of Neuroscience*, 36(33), 8653–8667. <https://doi.org/10.1523/jneurosci.1429-16.2016>
- Eitan, E., Green, J., Bodogai, M., Mode, N. A., Baek, R., Jorgensen, M. M., Freeman, D. W., Witwer, K. W., Zonderman, A. B., Biragyn, A., Mattson, M. P., Noren Hooten, N., & Evans, M. K. (2017). Age-related changes in plasma extracellular vesicle characteristics and internalization by leukocytes. *Scientific Reports*, 7(1), 1342. <https://doi.org/10.1038/s41598-017-01386-z>
- d'Errico, P., Ziegler-Waldkirch, S., Aires, V., Hoffmann, P., Mezö, C., Erny, D., Monasor, L. S., Liebscher, S., Ravi, V. M., Joseph, K., Schnell, O., Kierdorf, K., Staszewski, O., Tahirovic, S., Prinz, M., & Meyer-Luehmann, M. (2022). Microglia contribute to the propagation of A $\beta$  into unaffected brain tissue. *Nature Neuroscience*, 25(1), 20–25. <https://doi.org/10.1038/s41593-021-00951-0>
- Fröhlich, D., Kuo, W. P., Frühbeis, C., Sun, J. J., Zehendner, C. M., Luhmann, H. J., Pinto, S., Toedling, J., Trotter, J., & Krämer-Albers, E. M. (2014). Multifaceted effects of oligodendroglial exosomes on neurons: Impact on neuronal firing rate, signal transduction and gene regulation. *Philosophical Transactions of the Royal Society of London. Series B: Biological Sciences*, 369(1652), 20130510. <https://doi.org/10.1098/rstb.2013.0510>
- Gabrielli, M., Prada, I., Joshi, P., Falcicchia, C., D'Arrigo, G., Rutigliano, G., Battocchio, E., Zenatelli, R., Tozzi, F., Radeghieri, A., Arancio, O., Origlia, N., & Verderio, C. (2022). Microglial large extracellular vesicles propagate early synaptic dysfunction in Alzheimer's disease. *Brain*, 145(8), 2849–2868. <https://doi.org/10.1093/brain/awac083>
- Galimberti, D., Venturelli, E., Fenoglio, C., Guidi, I., Villa, C., Bergamaschini, L., Cortini, F., Scalabrini, D., Baron, P., Vergani, C., Bresolin, N., & Scarpini, E. (2008). Intrathecal levels of IL-6, IL-11 and LIF in Alzheimer's disease and frontotemporal lobar degeneration. *Journal of Neurology*, 255(4), 539–544. <https://doi.org/10.1007/s00415-008-0737-6>
- Gauthier, S., Webster, C., Servaes, S., Morais, J. A., & Rosa-Neto, P. (2022). Life after diagnosis: Navigating treatment, care and support. *World Alzheimer Report 2022*.
- Goetzl, E. J., Mustapic, M., Kapogiannis, D., Eitan, E., Lobach, I. V., Goetzl, L., Schwartz, J. B., & Miller, B. L. (2016). Cargo proteins of plasma astrocyte-derived exosomes in Alzheimer's disease. *FASEB Journal*, 30(11), 3853–3859. <https://doi.org/10.1096/fj.201600756R>
- Grapp, M., Wrede, A., Schweizer, M., Hüwel, S., Galla, H.-J., Snaidero, N., Simons, M., Bückers, J., Low, P. S., Urlaub, H., Gärtner, J., & Steinfeld, R. (2013). Choroid plexus transcytosis and exosome shuttling deliver folate into brain parenchyma. *Nature Communications*, 4(1), 2123. <https://doi.org/10.1038/ncomms3123>
- Grupp, L., Wolburg, H., & Mack, A. F. (2010). Astroglial structures in the zebrafish brain. *Journal of Comparative Neurology*, 518(21), 4277–4287. <https://doi.org/10.1002/cne.22481>
- Haddad, M., Perrotte, M., Ben Khedher, M. R., Demongin, C., Lepage, A., Fülöp, T., & Ramassamy, C. (2019). Methylglyoxal and glyoxal as potential peripheral markers for MCI diagnosis and their effects on the expression of neurotrophic, inflammatory and neurodegenerative factors in neurons and in neuronal derived-extracellular vesicles. *International Journal of Molecular Sciences*, 20(19), 4906. <https://doi.org/10.3390/ijms20194906>
- Haddad, M., Perrotte, M., Ben Khedher, M. R., Madec, E., Lepage, A., Fülöp, T., & Ramassamy, C. (2021). Levels of receptor for advanced glycation end products and glyoxalase-1 in the total circulating extracellular vesicles from mild cognitive impairment and different stages of Alzheimer's disease patients. *Journal of Alzheimer's Disease*, 84(1), 227–237. <https://doi.org/10.3233/jad-210441>
- Haddad, M., Perrotte, M., Landri, S., Lepage, A., Fülöp, T., & Ramassamy, C. (2019). Circulating and extracellular vesicles levels of N-(1-Carboxymethyl)-L-Lysine (CML) differentiate early to moderate Alzheimer's disease. *Journal of Alzheimer's Disease*, 69(3), 751–762. <https://doi.org/10.3233/jad-181272>
- Halliday, M. R., Rege, S. V., Ma, Q., Zhao, Z., Miller, C. A., Winkler, E. A., & Zlokovic, B. V. (2016). Accelerated pericyte degeneration and blood-brain barrier breakdown in apolipoprotein E4 carriers with Alzheimer's disease. *Journal of Cerebral Blood Flow and Metabolism*, 36(1), 216–227. <https://doi.org/10.1038/jcbfm.2015.44>
- Han, F., Chen, J., Belkin-Rosen, A., Gu, Y., Luo, L., Buxton, O. M., & Liu, X., & the Alzheimer's Disease Neuroimaging Initiative. (2021). Reduced coupling between cerebrospinal fluid flow and global brain activity is linked to Alzheimer disease-related pathology. *PLoS Biology*, 19(6), e3001233. <https://doi.org/10.1371/journal.pbio.3001233>
- Hardy, J. (2006). A hundred years of Alzheimer's disease research. *Neuron*, 52(1), 3–13. <https://doi.org/10.1016/j.neuron.2006.09.016>
- Hardy, J., & Selkoe, D. J. (2002). The amyloid hypothesis of Alzheimer's disease: Progress and problems on the road to therapeutics. *Science*, 297(5580), 353–356. <https://doi.org/10.1126/science.1072994>
- Hayashi, Y., Takamiya, M., Jensen, P. B., Ojea-Jiménez, I., Claude, H., Antony, C., Kjaer-Sorensen, K., Grabher, C., Boesen, T., Gilliland, D., Oxvig, C., Strähle, U., & Weiss, C. (2020). Differential nanoparticle sequestration by macrophages and scavenger endothelial cells visualized in vivo in real-time and at ultrastructural resolution. *ACS Nano*, 14(2), 1665–1681. <https://doi.org/10.1021/acs.nano.9b07233>
- Heneka, M. T., Carson, M. J., El Khoury, J., Landreth, G. E., Brosseron, F., Feinstein, D. L., Jacobs, A. H., Wyss-Coray, T., Vitorica, J., Ransohoff, R. M., Herrup, K., Frautschy, S. A., Finsen, B., Brown, G. C., Verkhratsky, A., Yamanaka, K., Koistinaho, J., Latz, E., Halle, A., ... Kummer, M. P. (2015). Neuroinflammation in Alzheimer's disease. *Lancet Neurology*, 14(4), 388–405. [https://doi.org/10.1016/s1474-4422\(15\)70016-5](https://doi.org/10.1016/s1474-4422(15)70016-5)



- Henson, H. E., Parupalli, C., Ju, B., & Taylor, M. R. (2014). Functional and genetic analysis of choroid plexus development in zebrafish. *Frontiers in Neuroscience*, 8, 364–364. <https://doi.org/10.3389/fnins.2014.00364>
- Hickman, S. E., Allison, E. K., & Khoury, J. E. (2008). Microglial dysfunction and defective  $\beta$ -amyloid clearance pathways in aging Alzheimer's disease mice. *The Journal of Neuroscience*, 28(33), 8354–8360. <https://doi.org/10.1523/jneurosci.0616-08.2008>
- Htike, T. T., Mishra, S., Kumar, S., Padmanabhan, P., & Gulyás, B. (2019). Peripheral biomarkers for early detection of Alzheimer's and Parkinson's diseases. *Molecular Neurobiology*, 56(3), 2256–2277. <https://doi.org/10.1007/s12035-018-1151-4>
- Hyenne, V., Ghoroghi, S., Collot, M., Bons, J., Follain, G., Harlepp, S., Mary, B., Bauer, J., Mercier, L., Busnelli, I., Lefebvre, O., Fekonja, N., Garcia-Leon, M. J., Machado, P., Delalande, E., López, A. A., Silva, S. G., Verweij, F. J., van Niel, G., ... Goetz, J. G. (2019). Studying the fate of tumor extracellular vesicles at high spatiotemporal resolution using the zebrafish embryo. *Developmental Cell*, 48(4), 554–572.e7. <https://doi.org/10.1016/j.devcel.2019.01.014>
- Imai, T., Takahashi, Y., Nishikawa, M., Kato, K., Morishita, M., Yamashita, T., Matsumoto, A., Charoenviriyakul, C., & Takakura, Y. (2015). Macrophage-dependent clearance of systemically administered B16BL6-derived exosomes from the blood circulation in mice. *Journal of Extracellular Vesicles*, 4, 26238. <https://doi.org/10.3402/jev.v4.26238>
- Jeong, J. Y., Kwon, H. B., Ahn, J. C., Kang, D., Kwon, S. H., Park, J. A., & Kim, K. W. (2008). Functional and developmental analysis of the blood-brain barrier in zebrafish. *Brain Research Bulletin*, 75(5), 619–628. <https://doi.org/10.1016/j.brainresbull.2007.10.043>
- Jin, S. W., Beis, D., Mitchell, T., Chen, J. N., & Stainier, D. Y. (2005). Cellular and molecular analyses of vascular tube and lumen formation in zebrafish. *Development*, 132(23), 5199–5209. <https://doi.org/10.1242/dev.02087>
- Kamrkar, S., LeBleu, V. S., Sugimoto, H., Yang, S., Ruivo, C. F., Melo, S. A., Lee, J. J., & Kalluri, R. (2017). Exosomes facilitate therapeutic targeting of oncogenic KRAS in pancreatic cancer. *Nature*, 546(7659), 498–503. <https://doi.org/10.1038/nature22341>
- Kerris, E. W. J., Hoptay, C., Calderon, T., & Freishtat, R. J. (2020). Platelets and platelet extracellular vesicles in hemostasis and sepsis. *Journal of Investigative Medicine*, 68(4), 813–820. <https://doi.org/10.1136/jim-2019-001195>
- Kimmel, C. B., Ballard, W. W., Kimmel, S. R., Ullmann, B., & Schilling, T. F. (1995). Stages of embryonic development of the zebrafish. *Developmental Dynamics*, 203(3), 253–310. <https://doi.org/10.1002/aja.1002030302>
- Koto, T., Takubo, K., Ishida, S., Shinoda, H., Inoue, M., Tsubota, K., Okada, Y., & Ikeda, E. (2007). Hypoxia disrupts the barrier function of neural blood vessels through changes in the expression of claudin-5 in endothelial cells. *The American Journal of Pathology*, 170(4), 1389–1397. <https://doi.org/10.2353/ajpath.2007.060693>
- Kur, I.-M., Prouvot, P.-H., Fu, T., Fan, W., Müller-Braun, F., Das, A., Das, S., Deller, T., Roeper, J., Stroth, A., & Momma, S. (2020). Neuronal activity triggers uptake of hematopoietic extracellular vesicles in vivo. *PLoS Biology*, 18(3), e3000643. <https://doi.org/10.1371/journal.pbio.3000643>
- Le Page, A., Dupuis, G., Frost, E. H., Larbi, A., Pawelec, G., Witkowski, J. M., & Fulop, T. (2018). Role of the peripheral innate immune system in the development of Alzheimer's disease. *Experimental Gerontology*, 107, 59–66. <https://doi.org/10.1016/j.exger.2017.12.019>
- Li, G., Simon, M. J., Cancel, L. M., Shi, Z. D., Ji, X., Tarbell, J. M., Morrison, B., III, & Fu, B. M. (2010). Permeability of endothelial and astrocyte cocultures: In vitro blood-brain barrier models for drug delivery studies. *Annals of Biomedical Engineering*, 38(8), 2499–2511. <https://doi.org/10.1007/s10439-010-0023-5>
- Licastro, F., Pedrini, S., Caputo, L., Annoni, G., Davis, L. J., Ferri, C., Casadei, V., & Grimaldi, L. M. (2000). Increased plasma levels of interleukin-1, interleukin-6 and alpha-1-antichymotrypsin in patients with Alzheimer's disease: Peripheral inflammation or signals from the brain? *Journal of Neuroimmunology*, 103(1), 97–102. [https://doi.org/10.1016/s0165-5728\(99\)00226-x](https://doi.org/10.1016/s0165-5728(99)00226-x)
- Lin, H., Dixon, S. G., Hu, W., Hamlett, E. D., Jin, J., Ergul, A., & Wang, G. Y. (2022). p38 MAPK is a major regulator of amyloid beta-induced IL-6 expression in human microglia. *Molecular Neurobiology*, 59(9), 5284–5298. <https://doi.org/10.1007/s12035-022-02909-0>
- Liu, R., Collier, J. M., Abdul-Rahman, N. H., Capuk, O., Zhang, Z., & Begum, G. (2024). Dysregulation of ion channels and transporters and blood-brain barrier dysfunction in Alzheimer's disease and vascular dementia. *Aging and Disease*, 15(4), 1748–1770. <https://doi.org/10.14336/ad.2023.1201>
- Long, X., Yao, X., Jiang, Q., Yang, Y., He, X., Tian, W., Zhao, K., & Zhang, H. (2020). Astrocyte-derived exosomes enriched with miR-873a-5p inhibit neuroinflammation via microglia phenotype modulation after traumatic brain injury. *Journal of Neuroinflammation*, 17(1), 89. <https://doi.org/10.1186/s12974-020-01761-0>
- Lyra E Silva, N. M., Gonçalves, R. A., Pascoal, T. A., Lima-Filho, R. A. S., Resende, E. d. P. F., Vieira, E. L. M., Teixeira, A. L., de Souza, L. C., Peny, J. A., Fortuna, J. T. S., Furigo, I. C., Hashiguchi, D., Miya-Coreixas, V. S., Clarke, J. R., Abisambra, J. F., Longo, B. M., Donato, J., Fraser, P. E., Rosa-Neto, P., ... De Felice, F. G. (2021). Pro-inflammatory interleukin-6 signaling links cognitive impairments and peripheral metabolic alterations in Alzheimer's disease. *Translational Psychiatry*, 11(1), 251. <https://doi.org/10.1038/s41398-021-01349-z>
- Marioni, R. E., Harris, S. E., Zhang, Q., McRae, A. F., Hagenaars, S. P., Hill, W. D., Davies, G., Ritchie, C. W., Gale, C. R., Starr, J. M., Goate, A. M., Porteous, D. J., Yang, J., Evans, K. L., Deary, I. J., Wray, N. R., & Visscher, P. M. (2018). GWAS on family history of Alzheimer's disease. *Translational Psychiatry*, 8(1), 99. <https://doi.org/10.1038/s41398-018-0150-6>
- Matsumoto, A., Takahashi, Y., Chang, H.-Y., Wu, Y.-W., Yamamoto, A., Ishihama, Y., & Takakura, Y. (2020). Blood concentrations of small extracellular vesicles are determined by a balance between abundant secretion and rapid clearance. *Journal of Extracellular Vesicles*, 9(1), 1696517. <https://doi.org/10.1080/20013078.2019.1696517>
- Matsumoto, J., Stewart, T., Sheng, L., Li, N., Bullock, K., Song, N., Shi, M., Banks, W. A., & Zhang, J. (2017). Transmission of  $\alpha$ -synuclein-containing erythrocyte-derived extracellular vesicles across the blood-brain barrier via adsorptive mediated transcytosis: Another mechanism for initiation and progression of Parkinson's disease? *Acta Neuropathologica Communications*, 5(1), 71. <https://doi.org/10.1186/s40478-017-0470-4>
- McGeer, P. L., & McGeer, E. G. (2013). The amyloid cascade-inflammatory hypothesis of Alzheimer disease: Implications for therapy. *Acta Neuropathologica*, 126(4), 479–497. <https://doi.org/10.1007/s00401-013-1177-7>
- Morad, G., Carman, C. V., Hagedorn, E. J., Perlin, J. R., Zon, L. I., Mustafaoglu, N., Park, T. E., Ingber, D. E., Daisy, C. C., & Moses, M. A. (2019). Tumor-derived extracellular vesicles breach the intact blood-brain barrier via transcytosis. *ACS Nano*, 13(12), 13853–13865. <https://doi.org/10.1021/acsnano.9b04397>
- Morales-Prieto, D. M., Murrieta-Coxca, J. M., Stojiljkovic, M., Diezel, C., Streicher, P. E., Henao-Restrepo, J. A., Röstel, F., Lindner, J., Witte, O. W., Weis, S., Schmeer, C., & Marz, M. (2022). Small extracellular vesicles from peripheral blood of aged mice pass the blood-brain barrier and induce glial cell activation. *Cells*, 11(4), 625. <https://doi.org/10.3390/cells11040625>
- Moss, C. E., Phipps, H., Wilson, H. L., & Kiss-Toth, E. (2023). Markers of the ageing macrophage: A systematic review and meta-analysis. *Frontiers in Immunology*, 14, 1222308. <https://doi.org/10.3389/fimmu.2023.1222308>
- Mulcahy, L. A., Pink, R. C., & Carter, D. R. (2014). Routes and mechanisms of extracellular vesicle uptake. *Journal of Extracellular Vesicles*, 3, 24641. <https://doi.org/10.3402/jev.v3.24641>
- Nair, A. L., Groenendijk, L., Overdeest, R., Fowke, T. M., Annida, R., Mocellin, O., de Vries, H. E., & Wevers, N. R. (2023). Human BBB-on-a-chip reveals barrier disruption, endothelial inflammation, and T cell migration under neuroinflammatory conditions. *Frontiers in Molecular Neuroscience*, 16, 1250123. <https://doi.org/10.3389/fnmol.2023.1250123>

- Nation, D. A., Sweeney, M. D., Montagne, A., Sagare, A. P., D'Orazio, L. M., Pachicano, M., Sepeshband, F., Nelson, A. R., Buennagel, D. P., Harrington, M. G., Benzinger, T. L. S., Fagan, A. M., Ringman, J. M., Schneider, L. S., Morris, J. C., Chui, H. C., Law, M., Toga, A. W., & Zlokovic, B. V. (2019). Blood-brain barrier breakdown is an early biomarker of human cognitive dysfunction. *Nature Medicine*, 25(2), 270–276. <https://doi.org/10.1038/s41591-018-0297-y>
- Ng, T. P., Feng, L., Nyunt, M. S., Feng, L., Gao, Q., Lim, M. L., Collinson, S. L., Chong, M. S., Lim, W. S., Lee, T. S., Yap, P., & Yap, K. B. (2016). Metabolic syndrome and the risk of mild cognitive impairment and progression to dementia: Follow-up of the Singapore Longitudinal Ageing Study Cohort. *JAMA Neurology*, 73(4), 456–463. <https://doi.org/10.1001/jamaneurol.2015.4899>
- Ngolab, J., Trinh, I., Rockenstein, E., Mante, M., Florio, J., Trejo, M., Masliah, D., Adame, A., Masliah, E., & Rissman, R. A. (2017). Brain-derived exosomes from dementia with Lewy bodies propagate  $\alpha$ -synuclein pathology. *Acta Neuropathologica Communications*, 5(1), 46. <https://doi.org/10.1186/s40478-017-0445-5>
- Nielsen, J. E., Honoré, B., Vestergård, K., Maltesen, R. G., Christiansen, G., Bøge, A. U., Kristensen, S. R., & Pedersen, S. (2021). Shotgun-based proteomics of extracellular vesicles in Alzheimer's disease reveals biomarkers involved in immunological and coagulation pathways. *Scientific Reports*, 11(1), 18518. <https://doi.org/10.1038/s41598-021-97969-y>
- Noe, C. R., Noe-Letschnig, M., Handschuh, P., Noe, C. A., & Lanzenberger, R. (2020). Dysfunction of the blood-brain barrier—A key step in neurodegeneration and dementia. *Frontiers in Aging Neuroscience*, 12, 185. <https://doi.org/10.3389/fnagi.2020.00185>
- Oliveira Silva, R., Counil, H., Rabanel, J. M., Haddad, M., Zauouter, C., Ben Khedher, M. R., Patten, S. A., & Ramassamy, C. (2024). Donepezil-loaded nanocarriers for the treatment of Alzheimer's disease: Superior efficacy of extracellular vesicles over polymeric nanoparticles. *International Journal of Nanomedicine*, 19, 1077–1096. <https://doi.org/10.2147/ijn.S449227>
- Park, H.-C., Kim, C.-H., Bae, Y.-K., Yeo, S.-Y., Kim, S.-H., Hong, S.-K., Shin, J., Yoo, K.-W., Hibi, M., Hirano, T., Miki, N., Chitnis, A. B., & Huh, T.-L. (2000). Analysis of upstream elements in the HuC promoter leads to the establishment of transgenic zebrafish with fluorescent neurons. *Developmental Biology*, 227(2), 279–293. <https://doi.org/10.1006/dbio.2000.9898>
- Park, J. S., Choe, K., Khan, A., Jo, M. H., Park, H. Y., Kang, M. H., Park, T. J., & Kim, M. O. (2023). Establishing co-culture blood-brain barrier models for different neurodegeneration conditions to understand its effect on BBB integrity. *International Journal of Molecular Sciences*, 24(6), 5283. <https://www.mdpi.com/1422-0067/24/6/5283>
- Pascual, M., Ibáñez, F., & Guerri, C. (2020). Exosomes as mediators of neuron-glia communication in neuroinflammation. *Neural Regeneration Research*, 15(5), 796–801. <https://doi.org/10.4103/1673-5374.268893>
- Pauwels, M. J., Xie, J., Ceroi, A., Balusu, S., Castelein, J., Van Wonterghem, E., Van Imschoot, G., Ward, A., Menheniott, T. R., Gustafsson, O., Combes, F., El Andaloussi, S., Sanders, N. N., Mäger, I., Van Hoecke, L., & Vandenbroucke, R. E. (2022). Choroid plexus-derived extracellular vesicles exhibit brain targeting characteristics. *Biomaterials*, 290, 121830. <https://doi.org/10.1016/j.biomaterials.2022.121830>
- Perets, N., Betzer, O., Shapira, R., Brenstein, S., Angel, A., Sadan, T., Ashery, U., Popovtzer, R., & Offen, D. (2019). Golden exosomes selectively target brain pathologies in neurodegenerative and neurodevelopmental disorders. *Nano Letters*, 19(6), 3422–3431. <https://doi.org/10.1021/acs.nanolett.8b04148>
- Perez-Gonzalez, R., Gauthier, S. A., Kumar, A., & Levy, E. (2012). The exosome secretory pathway transports amyloid precursor protein carboxyl-terminal fragments from the cell into the brain extracellular space. *Journal of Biological Chemistry*, 287(51), 43108–43115. <https://doi.org/10.1074/jbc.M112.404467>
- Perrotte, M., Haddad, M., Le Page, A., Frost, E. H., Fülöp, T., & Ramassamy, C. (2020). Profile of pathogenic proteins in total circulating extracellular vesicles in mild cognitive impairment and during the progression of Alzheimer's disease. *Neurobiology of Aging*, 86, 102–111. <https://doi.org/10.1016/j.neurobiolaging.2019.10.10>
- Rabanel, J.-M., Faivre, J., Zauouter, C., Patten, S. A., Banquy, X., & Ramassamy, C. (2021). Nanoparticle shell structural cues drive in vitro transport properties, tissue distribution and brain accessibility in zebrafish. *Biomaterials*, 277, 121085. <https://doi.org/10.1016/j.biomaterials.2021.121085>
- Rabanel, J.-M., Picc, P.-A., Landri, S., Patten, S. A., & Ramassamy, C. (2020). Transport of PEGylated-PLA nanoparticles across a blood brain barrier model, entry into neuronal cells and in vivo brain bioavailability. *Journal of Controlled Release*, 328, 679–695. <https://doi.org/10.1016/j.jconrel.2020.09.042>
- Rajendran, L., Honsho, M., Zahn, T. R., Keller, P., Geiger, K. D., Verkade, P., & Simons, K. (2006). Alzheimer's disease beta-amyloid peptides are released in association with exosomes. *Proceedings of the National Academy of Sciences*, 103(30), 11172–11177. <https://doi.org/10.1073/pnas.0603838103>
- Raponi, E., Agenes, F., Delphin, C., Assard, N., Baudier, J., Legraverend, C., & Deloulme, J.-C. (2007). S100B expression defines a state in which GFAP-expressing cells lose their neural stem cell potential and acquire a more mature developmental stage. *Glia*, 55(2), 165–177. <https://doi.org/10.1002/glia.20445>
- Ridder, K., Keller, S., Dams, M., Rupp, A. K., Schlaudraff, J., Del Turco, D., Starmann, J., Macas, J., Karpova, D., Devraj, K., Depboylu, C., Landfried, B., Arnold, B., Plate, K. H., Höglinger, G., Sültmann, H., Altevogt, P., & Momma, S. (2014). Extracellular vesicle-mediated transfer of genetic information between the hematopoietic system and the brain in response to inflammation. *PLoS Biology*, 12(6), e1001874. <https://doi.org/10.1371/journal.pbio.1001874>
- Rothaug, M., Becker-Pauly, C., & Rose-John, S. (2016). The role of interleukin-6 signaling in nervous tissue. *Biochimica et Biophysica Acta (BBA)—Molecular Cell Research*, 1863(6, Pt A), 1218–1227. <https://doi.org/10.1016/j.bbamcr.2016.03.018>
- Ruan, Z., Pathak, D., Venkatesan Kalavai, S., Yoshii-Kitahara, A., Muraoka, S., Bhatt, N., Takamatsu-Yukawa, K., Hu, J., Wang, Y., Hersh, S., Ericsson, M., Gorantla, S., Gendelman, H. E., Kaye, R., Ikezu, S., Luebke, J. I., & Ikezu, T. (2021). Alzheimer's disease brain-derived extracellular vesicles spread tau pathology in interneurons. *Brain*, 144(1), 288–309. <https://doi.org/10.1093/brain/awaa376>
- Saeedi, S., Israel, S., Nagy, C., & Turecki, G. (2019). The emerging role of exosomes in mental disorders. *Translational Psychiatry*, 9(1), 122. <https://doi.org/10.1038/s41398-019-0459-9>
- Šimić, G., Španić, E., Langer Horvat, L., & Hof, P. R. (2019). Blood-brain barrier and innate immunity in the pathogenesis of Alzheimer's disease. *Progress in Molecular Biology and Translational Science*, 168, 99–145. <https://doi.org/10.1016/bs.pmbts.2019.06.003>
- Sardar Sinha, M., Ansell-Schultz, A., Civitelli, L., Hildesjö, C., Larsson, M., Lannfelt, L., Ingelsson, M., & Hallbeck, M. (2018). Alzheimer's disease pathology propagation by exosomes containing toxic amyloid-beta oligomers. *Acta Neuropathologica*, 136(1), 41–56. <https://doi.org/10.1007/s00401-018-1868-1>
- Solana, R., Tarazona, R., Gayoso, I., Lesur, O., Dupuis, G., & Fulop, T. (2012). Innate immunosenescence: Effect of aging on cells and receptors of the innate immune system in humans. *Seminars in Immunology*, 24(5), 331–341. <https://doi.org/10.1016/j.smim.2012.04.008>
- Stine, W. B., Jungbauer, L., Yu, C., & LaDu, M. J. (2011). Preparing synthetic A $\beta$  in different aggregation states. *Methods in Molecular Biology*, 670, 13–32. [https://doi.org/10.1007/978-1-60761-744-0\\_2](https://doi.org/10.1007/978-1-60761-744-0_2)
- Sun, J., Ou, W., Han, D., Paganini-Hill, A., Fisher, M. J., & Sumbria, R. K. (2022). Comparative studies between the murine immortalized brain endothelial cell line (bEnd.3) and induced pluripotent stem cell-derived human brain endothelial cells for paracellular transport. *PLoS ONE*, 17(5), e0268860. <https://doi.org/10.1371/journal.pone.0268860>
- Swardfager, W., Lanctôt, K., Rothenburg, L., Wong, A., Cappell, J., & Herrmann, N. (2010). A meta-analysis of cytokines in Alzheimer's disease. *Biological Psychiatry*, 68(10), 930–941. <https://doi.org/10.1016/j.biopsych.2010.06.012>
- Tóth, E., Turiák, L., Visnovitz, T., Cserép, C., Mázl, A., Sódar, B. W., Försönits, A. I., Petővári, G., Sebestyén, A., Komlósi, Z., Drahos, L., Kittel, Á., Nagy, G., Bácsi, A., Dénes, Á., Gho, Y. S., Szabó-Taylor, K., & Buzás, E. I. (2021). Formation of a protein corona on the surface of extracellular vesicles in blood plasma. *Journal of Extracellular Vesicles*, 10(11), e12140. <https://doi.org/10.1002/jev2.12140>

- van Lessen, M., Shibata-Germanos, S., van Impel, A., Hawkins, T. A., Rihel, J., & Schulte-Merker, S. (2017). Intracellular uptake of macromolecules by brain lymphatic endothelial cells during zebrafish embryonic development. *eLife*, 6, e25932. <https://doi.org/10.7554/eLife.25932>
- van Niel, G., D'Angelo, G., & Raposo, G. (2018). Shedding light on the cell biology of extracellular vesicles. *Nature Reviews Molecular Cell Biology*, 19(4), 213–228. <https://doi.org/10.1038/nrm.2017.125>
- Varga, Z., Gyurkó, I., Pálóczi, K., Buzás, E. I., Horváth, I., Hegedűs, N., Máthé, D., & Szigeti, K. (2016). Radiolabeling of extracellular vesicles with (99m)Tc for quantitative in vivo imaging studies. *Cancer Biotherapy and Radiopharmaceuticals*, 31(5), 168–173. <https://doi.org/10.1089/cbr.2016.2009>
- Vaz, R., Hofmeister, W., & Lindstrand, A. (2019). Zebrafish models of neurodevelopmental disorders: Limitations and benefits of current tools and techniques. *International Journal of Molecular Sciences*, 20(6), 1296. <https://doi.org/10.3390/ijms20061296>
- Visconte, C., Golia, M. T., Fenoglio, C., Serpente, M., Gabrielli, M., Arcaro, M., Sorrentino, F., Busnelli, M., Arighi, A., Fumagalli, G., Rotondo, E., Rossi, P., Arosio, B., Scarpini, E., Verderio, C., & Galimberti, D. (2023). Plasma microglial-derived extracellular vesicles are increased in frail patients with Mild Cognitive Impairment and exert a neurotoxic effect. *Geroscience*, 45(3), 1557–1571. <https://doi.org/10.1007/s11357-023-00746-0>
- Wang, J. H., Wu, Y. J., Tee, B. L., & Lo, R. Y. (2018). Medical comorbidity in Alzheimer's disease: A nested case-control study. *Journal of Alzheimer's Disease*, 63(2), 773–781. <https://doi.org/10.3233/jad-170786>
- Wang, Y., Balaji, V., Kaniyappan, S., Krüger, L., Irsen, S., Tepper, K., Chandupatla, R., Maetzler, W., Schneider, A., Mandelkow, E., & Mandelkow, E. M. (2017). The release and trans-synaptic transmission of Tau via exosomes. *Molecular Neurodegeneration*, 12(1), 5. <https://doi.org/10.1186/s13024-016-0143-y>
- Welsh, J. A., Goberdhan, D. C. I., O'Driscoll, L., Buzas, E. I., Blenkiron, C., Bussolati, B., Cai, H., Di Vizio, D., Driedonks, T. A. P., Erdbrügger, U., Falcon-Perez, J. M., Fu, Q. L., Hill, A. F., Lenassi, M., Lim, S. K., Mahoney, M. G., Mohanty, S., Möller, A., Nieuwland, R., ... Witwer, K. W. (2024). Minimal information for studies of extracellular vesicles (MISEV2023): From basic to advanced approaches. *Journal of Extracellular Vesicles*, 13(2), e12404. <https://doi.org/10.1002/jev2.12404>
- West, P. K., McCorkindale, A. N., Guennewig, B., Ashhurst, T. M., Viengkhou, B., Hayashida, E., Jung, S. R., Butovsky, O., Campbell, I. L., & Hofer, M. J. (2022). The cytokines interleukin-6 and interferon- $\alpha$  induce distinct microglia phenotypes. *Journal of Neuroinflammation*, 19(1), 96. <https://doi.org/10.1186/s12974-022-02441-x>
- Wright, R. (2021). Microglia set the pace for tau spread. *Nature Neuroscience*, 24(10), 1342–1342. <https://doi.org/10.1038/s41593-021-00931-4>
- Xia, Y., Zhang, G., Han, C., Ma, K., Guo, X., Wan, F., Kou, L., Yin, S., Liu, L., Huang, J., Xiong, N., & Wang, T. (2019). Microglia as modulators of exosomal alpha-synuclein transmission. *Cell Death and Disease*, 10(3), 174. <https://doi.org/10.1038/s41419-019-1404-9>
- Xie, J., Van Hoecke, L., & Vandenbroucke, R. E. (2021). The impact of systemic inflammation on Alzheimer's disease pathology. *Frontiers in Immunology*, 12, 796867. <https://doi.org/10.3389/fimmu.2021.796867>
- Zheng, T., Pu, J., Chen, Y., Guo, Z., Pan, H., Zhang, L., Zhang, H., Sun, B., & Zhang, B. (2017). Exosomes secreted from HEK293-APP Swe/Ind cells impair the hippocampal neurogenesis. *Neurotoxicity Research*, 32(1), 82–93. <https://doi.org/10.1007/s12640-017-9713-1>
- Zhou, W., Fong, M. Y., Min, Y., Somlo, G., Liu, L., Palomares, M. R., Yu, Y., Chow, A., O'Connor, S. T. F., Chin, A. R., Yen, Y., Wang, Y., Marcusson, E. G., Chu, P., Wu, J., Wu, X., Li, A. X., Li, Z., Gao, H., ... Wang, S. E. (2014). Cancer-secreted miR-105 destroys vascular endothelial barriers to promote metastasis. *Cancer Cell*, 25(4), 501–515. <https://doi.org/10.1016/j.ccr.2014.03.007>

## SUPPORTING INFORMATION

Additional supporting information can be found online in the Supporting Information section at the end of this article.

**How to cite this article:** Counil, H., Silva, R. O., Rabanel, J.-M., Zaouter, C., Haddad, M., Ben Khedher, M. R., Brambilla, D., Fülöp, T., Patten, S. A., & Ramassamy, C. (2025). Brain penetration of peripheral extracellular vesicles from Alzheimer's patients and induction of microglia activation. *Journal of Extracellular Biology*, 4, e70027. <https://doi.org/10.1002/jex2.70027>